

A CHRONOSEQUENCE OF CRACKING IN MILL CREEK, CALIFORNIA

by

Samantha Berberich

A thesis submitted to the faculty of The University of North Carolina at  
Charlotte in partial fulfillment of the requirements for the degree of Master  
of Science in Earth Sciences Charlotte 2020

Approved by:

---

Dr. Martha-Cary Eppes

---

Dr. Andy Bobyarchick

---

Dr. Brian Magi

©2020  
Samantha Berberich  
ALL RIGHTS RESERVED

## ABSTRACT

SAMANTHA BERBERICH. A Chronosequence of Cracking in Mill Creek, California. (Under the direction of DR. MARTHA CARY EPPES)

Mechanical weathering –aka physical weathering; the process by which rock is broken down into smaller pieces --is one of the first modifications rock undergoes once it approaches Earth's surface. Essentially, almost all processes that shape the landscape can't occur without mechanical weathering. Cracking is one form of weathering, but before we can completely understand any surficial process that is predicated on rock cracking, we must characterize and understand cracking itself. How cracking changes and affects rocks through time is a feature of physical weathering that is relatively unknown compared to chemical weathering. I hypothesize that mechanical weathering rates will initially be fast, with a sharp increase in the size and numbers of cracks, followed by a period in which crack size and numbers plateau. This hypothesis was tested through the collection of crack characteristic data – length, width, density, and a variety of other rock and crack metrics that provide insight into both the style and rate of cracking. Data were collected from boulders naturally deposited on the surface of glacial moraines and stream floodplains and terraces on the eastern flank of Sierra Nevada Mountains, in the vicinity of Mono Lake, in California. Previously these surfaces had been dated by Rood (2011) using measurements of  $^{10}\text{Be}$  on the surface of large ( $>1$  m) boulders found on the surfaces. The surfaces studied here included a streambed, referred to as the

“Modern Wash” at 0 years, and a Holocene age terrace (with an estimated age of 5000 years), and five more surfaces that had been previously dated. The average exposure ages of these surfaces previously calculated by Rood (2011) were as follows; Lundy Canyon Outwash Terrace: 40 ka, Lundy Canyon Moraine: 19 ka, Mono Basin Moraine: 40 ka, Buckeye Creek Outwash Terrace: 227 ka, and Sherwin Moraine: 77 ka. In this study, I collected data both on “dated boulders” – the large boulders that Rood (2011) had sampled, as well as “transect boulders” – a set of 100 clasts that were identified on each of 5 surfaces. Boulders were selected on a size criteria, the length had to be greater than 15 cm, but no more than 50 cm. For each of the “dated boulders” crack data was collected from 20x20 cm representative squares drawn on the boulder. For each transect boulder, crack data was collected for all cracks found in the 100 boulder transect. Results suggest that more recently exposed rock deposits from the Holocene Outwash Terrace display higher crack densities and crack lengths than the rocks on the older surfaces. Using dimensional data for both the boulders themselves and the cracks on them, a trend was able to be seen.

For most of the variables data was collected on, crack length, width, density, etc. a spike in these variables was seen around 5000 years, followed by an immediate decline and gradual plateau as the surfaces got older. For the other, non-crack specific data, a similar, if slightly less defined time trend can also be seen. This result does not disprove the initial hypothesis, rather it highlights the idea that cracks can disappear through time as pieces fall off boulders. In sum, rates of rock cracking appear to decrease through time as the rock is exhumed. These results have important implications for understanding the effect of mechanical weathering on rocks both out in nature and ones used for building within our cities.

## TABLE OF CONTENTS

LIST OF TABLES	vi
LIST OF FIGURES	vii
CHAPTER 1: INTRODUCTION	1
CHAPTER 2: BACKGROUND	3
2.1. Mechanical Weathering Overview	3
2.2. Crack Morphology in Boulders	3
2.3. Sources of Environmental Stress	4
2.4. Weathering-Related Bond Breaking Processes	9
2.5. Chronosequences	12
CHAPTER 3: STUDY AREA	21
3.1. Geomorphology of the Mono Basin	14
3.2. Paleoclimate and Modern Climate	18
CHAPTER 4: METHODS	21
4.1. Dated Boulder Collection	21
4.2. Transect Boulder Collection	23
4.3. Crack Measurements – Dated and Transect Boulders	24
4.4. Crack Density Calculation	27
4.5. Thin Section Analysis	27
CHAPTER 5: RESULTS	29
5.1. Rock and Crack Characteristics by Exposure Age	29
5.2. Chronofunction of Rock and Crack Data	35
CHAPTER 6: DISCUSSION	39
CHAPTER 7: CONCLUSION	43
REFERENCES	45

## LIST OF TABLES

TABLE 1: Basic Surface Characteristics for all seven surfaces	68
TABLE 2: Dated Boulders and their Crack Characteristics	69
TABLE 3: Transect Boulders and their Crack Characteristics	71
TABLE 4: Sample Thin Section Point Counts	73
TABLE 5: Differences in lichen and varnish for Transect Boulders	76
TABLE 6: Number of Transect Boulders in each Embeddedness Category	76
TABLE 7: Crack Type Counts for All Surfaces	76
TABLE 8: Cracks less than 2 centimeters for Sampled Surfaces	77
TABLE 9: Granular Disintegration Counts for Sampled Rocks	77

## LIST OF FIGURES

FIGURE 1: Conceptual graph of Mechanical Weathering over time	78
FIGURE 2: Illustrated bond breaking process of subcritical cracking	79
FIGURE 3: Common types of crack morphology	80
FIGURE 4: Watershed map of Mill Creek Drainage Basin	81
FIGURE 5: Map of sample site locations in relation to each other	82
FIGURE 6: Topographic maps taken from Rood 2011	83
FIGURE 7: Satellite photos of samples surfaces	84
FIGURE 8: Photos of each sample location	85
FIGURE 9: Example of a previously sampled dated boulder	86
FIGURE 10: Sphericity and Roundness Chart	87
FIGURE 11: Example of placement of representative boxes on boulders	88
FIGURE 12: Embeddedness scale and crack weathering index	89
FIGURE 13: Dimensions of Dated Boulders based on approximate ages	90
FIGURE 14: Dimensions of Transect Boulders based on approximate ages	91
FIGURE 15: Sphericity and Angularity of Transect Boulders for each surface	92
FIGURE 16: Quadruple graph of various boulder characteristics	93
FIGURE 17: Crack dimensions for Dated Boulders	94
FIGURE 18: Crack dimensions for Transect Boulders	95
FIGURE 19: Crack density for Transect Boulders	96
FIGURE 20: Log of crack density for Dated Boulders	97
FIGURE 21: Percentage of each crack type on all surfaces	98
FIGURE 22: Rose diagrams for Transect Boulder strikes	99
FIGURE 23: Rose diagrams for Dated Boulder strikes	99
FIGURE 24: Rose diagrams for Transect Boulder dips	100
FIGURE 25: Rose diagrams for Dated Boulder dips	100

FIGURE 26: Average strike/dip for Transect and Dated Boulders	101
FIGURE 27: Example of a “daughter boulder”	102



## CHAPTER 1: INTRODUCTION

Mechanical weathering – aka physical weathering; the process by which rock is broken down into smaller pieces - is one of the first modifications rock undergoes as it is exhumed. Essentially, almost all processes that shape landscapes cannot occur without mechanical weathering. Mechanical weathering in rock starts with ‘inherent weaknesses’ that can be anything from a small pore space, to a weaker mineral contained within the larger rock, or even a change in the composition of the rock from layer to layer. When these heterogeneities undergo stresses, they tend to concentrate even the very low stresses, (Eppes and Keanini, 2017, Anderson, 2005), causing the weakness to propagate as a crack – a planar void in the rock. Cracks that appear as a result of these inherent weaknesses and subsequent stresses are what constitutes mechanical weathering. Cracking contributes to processes ranging from the formation of exfoliation sheets in the granite domes of Yosemite (Collins et al., 2018), to the erosion of the rock fragments that eventually go on to compose soil (Scarciglia et al., 2005), to the erosion of the Appalachian Mountains (Hancock, 2007). Thus, before we can completely understand any surficial process involving rock cracking, we must characterize and understand cracking itself. In addition to shedding light on fundamental geologic processes, documenting and understanding natural crack propagation has direct applications to the preservation of historic and world heritage sites. For example, harsh cleaning of historic stone monuments and buildings is utilized to keep plant matter off the buildings. Studies have shown, however, that the growth of organic matter on historic buildings may actually help slow down the physical weathering by forming a support system within the building stones (Salvadori, 2016). Before we can take steps to slow down the weathering of historic sites, we need to fully understand the mechanical weathering of the rocks that comprise them.

Despite its overall importance, there are numerous tenants of physical weathering that geomorphologists take for granted. For example, deriving erosion rates from bare rock outcrops using cosmogenic beryllium 10 relies on the assumption that the rock being measured has eroded at a steady rate (e.g. Kirchner, 2001). But few if any studies have ever actually documented how such erosion proceeds through time (Mushkin et al., 2014). Thus, if physical weathering tends to slow or accelerate with time, such assumptions might be invalid.

The goal of this study is to better understand one component of mechanical weathering in nature, the connection between mechanical weathering and time. In this study, I document and quantify cracks on boulders found within different geomorphic surfaces (moraines and terraces) of known ages. As such, I develop a *chronosequence* – weathering characteristics described on a set of geologic surfaces that share a similar environment, but differ in exposure age - of mechanical weathering in order to document how the characteristics of rock cracking evolves with time. I hypothesize that, similar to chemical weathering, mechanical weathering progresses at a steady rate until easily weathered minerals have been exhausted, whereupon weathering rates will plateau (Figure 1). Thus, overall, with the collected chronosequence data, I will test the hypothesis that mechanical weathering rates are fastest upon initial exposure of the rock and slow with time. In doing so, I will provide a basic idea of how mechanical weathering proceeds over time, a previously unexplored process within the field of geomorphology.

## CHAPTER 2: BACKGROUND

### *2.1. Mechanical Weathering Background Overview*

Here I define mechanical weathering as any cracking that occurs in bedrock or a clastic sediment within roughly 100 meters of Earth's surface. In this study, I define a crack as any planar void within rock, meant as an observable feature unrelated to strain. Under this rule, not only are small, sub- mm voids considered, but also larger voids, which might be termed 'joints' or 'fractures' in other studies. In general, in order for any crack to form in rock, three things are required. First, a flaw of some sort needs to be present within the rock that can concentrate stress (see below). Such flaws include pores, inclusions or bedding planes. Next the rock must experience some type of mechanical stress loading that may include tectonic, topographic and environmental (thermal, freezing, and salt/mineral hydration) stresses. Lastly, due to this external stress-loading, molecular bonds within the rock – at the crack tip - need to break (Figure 2). In order to somewhat reduce the complications of multiple sources of stress on mechanical weathering, such as tectonic stresses or topographic stresses (such as that due to a large overlying mass of rock), this research will focus on boulders, not bedrock. Thus, the following background sections focus on the environmental stresses and bond- breaking processes likely to be experienced by boulders.

### *2.2. Crack Morphology in Boulders*

Based on existing literature that describes cracks in boulders, (e.g. Eppes et al., 2010, Aldred et al., 2016, Mc Fadden et al., 2005), there are three distinct categories of cracks that form in surface bedrock and/or boulders (Figure 3): 1) Intergranular cracks, which form along individual crystal or grain boundaries. This type of crack results in granular disintegration of the rock that forms grus, sand-gravel sized sediment

composed of individual rock crystals. The presence of *grus* is a key indicator that intergranular cracking is occurring in surrounding rocks 2) Surface parallel cracks, which are considered any crack parallel to the outside boundary of the rock they are on. The surface flake height that is dislodged by a surface-parallel crack – by convention - takes up no more than ten percent of the total height of the rock (arrow in Figure 3B), and 3) Through-going cracks, which do not follow any visible rock related features, but will eventually result in the rock splitting into two or more pieces. Any of these three types of cracks might – in turn – be parallel to rock features such as foliation, bedding or the longitudinal axis. To date, no study has systematically examined how these crack types change through time as a rock is exposed.

### *2.3. Sources of Environmental Stress*

#### *Thermal*

Rock that is exposed to the sun, either daily, or on shorter or longer timescales, undergoes thermal cycling, which can produce thermal stresses in rock. Most rocks world- wide are constantly exposed to thermal cycling throughout the course of the day and year, which can cause the crystals that make up the rocks to swell or contract in accordance with their coefficients of thermal expansion. There are two mechanistic origins of thermal stresses 1) intergranular thermal stresses and 2) rock-scale thermal stresses (Ravaji et al.2019). Intergranular stresses arise when grains located near each other have different coefficients of thermal expansion, leading to stresses at their boundaries. This stress can lead to intergranular style cracking. Whole-rock stresses arise when one portion of the rock is heated or cooled at a different rate from other parts of the rock, often caused by rapid changes in the surface temperature of the clast in question. This stress can result in surface parallel or through-going style cracks. Even though previous work has divided the types of thermal stress origins in two, in a real-life

field situation, there is little chance of differentiation, other than by the type of cracks that are forming.

Thermally driven cracking is documented to occur naturally in granite or granodiorite (Wang, 1989) as well as in marble (Luque et al., 2011), shale (Chen, 2003) and basalt (Valentine and Groves, 1996). Thermal stress magnitudes have been estimated to range from 0.05 to 0.7 MPa in rock (e.g. Eppes et al., 2016, Collins et al, 2017). In comparison to other sources of stress such as: freezing (1-8 MPa), hydration (0.4-0.8 MPa), and topographical compression (0.15-0.4 MPa) (Walder and Hallet, 1985; Bost and Pouya, 2016), thermal stresses have magnitudes on the smaller end. This may seem insignificant over a short period of time, but over the course of a year, for example, over 30,000 cracking events can occur in a boulder (Eppes et al., 2016). Thermally-induced cracking can also produce a distinct crack direction, related to the orientation of the sun (e.g. Eppes, et al, 2010). Rose diagrams of cracks within boulders show that many of the cracks appear to have a north-south, or meridional trend to them (e.g. Aldred et al., 2016, Eppes et al., 2015). This north-south trend provides strong evidence that those boulder cracks are related, in some way, to thermal stress – driven by how the sun moves in the sky east to west.

#### *Freeze/Thaw*

There are several avenues by which freezing water may create stresses. The most commonly cited is that due to cycles of freezing temperatures whereby, moisture in and around rocks freeze at a microscopic or even macroscopic level. The solidified water expands by 9% upon freezing, and then creates hydrostatic pressure up against the grains it is being held between. When that ice thaws, the pressure is rapidly released, with repeated cycles of freezing and thawing eventually loosening the grains from alternating effective tensile and compressive

stresses. The effect of these cycles starts out small, until micro-cracks propagate to planar fractures that become visible and start to slough off larger chunks of the rock (Halsey, 1998). The cracks observed to have formed from these freezing stresses within rocks do not normally occur as random fractures, instead they tend to follow grain boundaries and bedding planes (Cui, 2017). These types of boundaries are easy to exploit via mechanical weathering generally because they are already areas that concentrate stresses.

Another hypothesized mechanism by which freezing water may induce stress is dependent, not on repeated freeze/thaw cycles, but instead on the rate of water freezing within the rock (Izumiyama, 2012). This rapid freezing process has been shown to cause enough stress to create more pores, which allows for a higher porosity within the rock in question (Vlahou and Worster, 2015). This creation of pore space induces a positive feedback cycle where the increased pore space allows for further penetration into the rock by water, which then freezes and starts the process over again. Freeze cycle mechanisms do not always occur in short periods of time such as a diurnal freeze/thaw cycle. There are seasonal freezing cycles that occur over longer periods of time. These types fall into two categories; unilateral and bilateral (Murton et al., 2006). Unilateral freezing is associated with areas that undergo seasonal freezing, whereas bilateral freezing is associated with areas that contain permafrost year round. The two different types of freezing cycles lead to different stress states affecting rocks in the area. When caused by unilateral freezing, the resulting cracks propagate further from the surface. When caused by bilateral freezing, the cracks are restricted above the permafrost and are not as numerous as the unilateral cracks.

A final process of freezing-related stress is caused by ice segregation. During this process, water stored in capillaries and on mineral particles is squeezed into a porous medium like rock or soil due to temperature differences between the void spaces and the water itself. Due to thermodynamics, water moves towards areas at the crack tip where freezing is

occurring, causing the new water to freeze as well. Through this process, the fractures in which this newly frozen water is concentrated will buckle due to the stress exerted on it by the evergrowing solid lens of ice. The stresses associated with freezing – inclusive of all the above processes -- have been estimated to range from 0.1-7 Mpa (e.g. Walder and Hallet, 1985, Bost and Pouya, 2016).

### *Salt Precipitation*

Salt precipitation is the process by which salts present in the rock environment – dissolved in water and found in cracks or pores – crystalize as water evaporates. As new water moves in and more salts crystalize, pressure is transferred from the solid salts to the surrounding material. The precipitation of salt crystals can result from rapid fluctuations in either temperature or moisture. Within soil or at the surface of the earth is the best place to experience these changes (Amit, 1993). The resulting pressure from the salt crystals helps push the host rock apart, resulting in stresses that may be on the order of 1-13 Mpa (Sousa, 2018) and thus contribute to the mechanical weathering of the rock. Salt weathering can be commonly observed in urban areas, where the use of granites is prevalent as building and walkway material (Sousa, 2018). In these locations, the use of salts to stop ice from forming on city sidewalks is the direct source of the salt crystals that are found within the pore space of the rock. In natural environments, the salts are found as accessory minerals that compose rock.

Permeability and porosity are key factors that allow for the movements of dissolved salts within the structure of rock. The more permeable a rock is, the easier it is for liquid to be transported and forced into available pores through capillary action (Sousa, 2018). Larger pores that contain salt crystals have lower crystallization pressure than smaller pores, so if a rock has a high permeability, and high porosity, less weathering will occur

### *Mineral Hydration and Hydrolysis*

The hydration or hydrolysis of minerals within rock will also contribute to the formation of stress that can lead to cracking. Hydration of a mineral occurs when water is introduced into the chemical structure of the mineral, which creates a different mineral altogether. In the case of hydrolysis, with the addition of water to a mineral, its structure undergoes a chemical breakdown and converts the primary mineral into a secondary mineral. A common example of this is in weathered biotite, which chemically alters as it breaks down in the presence of water. This alteration changes the Fe(II) to Fe(III) within the crystal and causes the crystal to expand along cleavage planes, putting pressure on the surrounding grains, and commonly causing small cracks to form within them (Holbrook et al 2019). As with all of these stress-inducing processes, these neighboring cracks constitute voids within the rock where more water can enter and encourage weathering. Another example of mineral hydration causing stress is related to clay-cemented sandstones, whereby the grains themselves can be held together via a clay cement and can crack as the clay minerals are hydrated and then expand /contract. This expansion increases the amount of pore space within the sandstone upon drying, which again, allows more water to access the grains (Burnett, 2007). The hydration of salts already found within pore spaces can occur even in very cold environments, due to a continuous supply of water even when the ground itself is frozen over (Sousa, 2018). Stresses from mineral expansion have been estimated to be between 0.4-0.8 Mpa, all the way up to 27 Mpa (Lambart, 2018).

#### *2.3. Weathering-Related Bond Breaking Processes*

Bond breaking (hereafter cracking) within rocks can occur critically or subcritically. Critical cracking occurs when the stresses exerted on a brittle solid exceed the material's brittle strength, and cracks grow rapidly, and the material fails. A perfect example of this is the traditional 'breaking the wishbone' done at Thanksgiving. The force exerted by each person holding the wishbone is greater than the material's strength and it suddenly snaps.



Subcritical cracking is slow, stable cracking that occurs at stresses lower than the bulk strength of the material. A well-known example of this would be a crack growing over weeks in a car windshield. Upon the initial crack, the windshield does not shatter immediately, but over time, the small crack slowly propagates to span the entire windshield. Crack initiating stress magnitudes that have been calculated by researchers for environmental stresses are far lower than the critical strength of most rock masses (e.g. Eppes and Keanini, 2017). The reported tensile strengths of rock vary greatly; for example three common rock types; granite, sandstone, and limestone, have reported strengths as 13 MPa, 3-7 MPa, and 2.5-4 MPa respectively (Mingqing, 2015). The pressure needed for subcritical cracking, however, is much lower than the critical strength of most rocks (thought to be at least as low as 10% of the critical strength), therefore it is likely that most cracking in boulders is a result of subcritical cracking (Eppes and Keanini, 2017). Here I will assume that all cracking observed in boulders selected for this study occurs subcritically. Subcritical cracking is best understood in terms of the concept of stress intensity. Flaws within a brittle material amplify the external stresses applied to the solid and concentrate or amplify them directly at the crack tip. The amount of crack tip stress magnification, i.e. stress intensity, is proportional to both the external stress magnitude as well as the length of the crack. Thus, subcritical cracking occurs as a function of the stress intensity factor, defined most generically for tensile stresses as  $K_1 \approx \sigma \sqrt{\pi a}$ . The stress intensity factor incorporates two main variables:  $\sigma$ , which represents the stress caused by the external load, and  $a$ , which is one half the length of the crack in question (e.g. Eppes and Keanini, 2017).

Charles' Law is used to estimate subcritical cracking rates under different stress intensities. Charles' Law represents the velocity of crack propagation as being equal to the stress intensity experienced by any given crack divided by the fracture toughness (the critical stress intensity) of the material. This is represented in the formula (Formula 1)

below.

$$\text{Formula 1 } \frac{da}{dt} = A \left( \frac{k1c}{K1c} \right)^n \quad \text{—}$$

represents the velocity of the crack propagation, A represents a constant velocity that is true when  $\frac{k1c}{K1c}$  is equal to 1.  $\frac{k1c}{K1c}$  represents the stress intensity of a crack with a defined length, divided by the critical stress intensity, or the point at which the outside stress is greater than the fracture toughness of the rock – the critical stress intensity - the crack is within. This is all placed within parenthesis to the nth power, and exponent referred to as the “subcritical cracking index” (Atkinson, 1987). When the stress intensity on a crack is less than the fracture toughness, the crack will propagate subcritically at the calculated velocity. Because natural stresses experienced at Earth’s surface are low magnitude (Eppes et al., 2018), most of the stresses upon a rock are above the threshold for subcritical cracking, but below the threshold for the more obvious critical cracking. Over time, this slow cracking presumably adds up, and helps facilitate natural rock erosion. To date, no study has directly examined long- term subcritical cracking rates in rock.

Subcritical cracking can affect all types of rocks (Atkinson, 1984; Brantut et al., 2014; Nara et al., 2010, Meredith and Atkinson, 1985). The bond-breaking processes of subcritical cracking occur by chemical reactions between moisture found in the crack, and the rock or mineral itself (Figure 2). Within the rock, the bonds between elements found immediately at the crack tip are experiencing high stress intensity. Because of this tension, water molecules become reactive with the mineral or rock, which are weakened at the crack tip, where they are stretched by the stress. This reaction with water replaces the relatively strong bonds of the rock, with weaker hydrogen bonds from the water molecule, in that particular location, leading the crack to propagate at stress levels lower than the overall strength of the rock itself. Due to the fact that it is a chemical reaction that is taking place right at the crack tip,

variables that would affect chemical reactions also have an effect on subcritical cracking rates. These include the composition of the material undergoing the stress as well as environmental factors such as relative humidity and rock temperature. Theoretical modeling has shown that the cracking rate is directly related to these environmental factors (Eppes and Keanini, 2017). I hypothesize that cracking rates may therefore change as the climate of the environment changes, such as from glacial to interglacial periods. A wetter, warmer climate would traditionally result in faster cracking rates, while the cooler, drier glacial climate would not have cracks propagating at the same speed. I believe that these rates could differ due to the historical climate in the Mono Lake area, regardless of its glacial history.

#### *2.4. Chronosequences*

Within soil science, chronosequences are often used as a way to substitute “time” for “space” in order to understand how processes progress as deposits age and weather. Climate, organic lifeforms, topography, precipitation and time are all variables that can affect how rocks and sediment weather (Jenny, 1941). Chronosequences work by comparing groupings of differently aged soils or rocks that have developed under the influence of the same factors, i.e. the same parent materials, climate, and geomorphology. A chronosequence is based on the idea that all of the variables except time have remained constant for each of the observation sites within the chronosequence. Chronosequences can serve the function of estimating ages of deposits when variables other than time are similar (e.g. Eppes et al., 2008). They also can assist in learning about landscape development due to a changing climate or tectonic shifts (e.g. Layzell et al., 2012). In the case of this current study, the rocks of the chronosequence were deposited on the surface of a series of glacial moraines and fluvial terraces. The moraines in the Lundy Canyon location are what remain from several glaciation events, with a minimum of four individual glacial events represented (see below). As the deposits increase in age, under similar conditions, the assumption would be that weathering of any boulders found on the surface of the

deposits continues through time. The goal of this study is to assess how mechanical weathering changes over time, and the known ages of each moraine or fluvial terrace provide a time reference in which we can assess the extent of mechanical weathering rates. Two primary assumptions are involved in employing these deposits as a proxy for mechanical weathering as a function of time: 1) The extent and density of vegetation ground cover has not changed drastically between the geographic locations of the chronosequence, and 2) The erosion or lack thereof, where I am assuming that the rate of erosion of geomorphic surfaces has stayed constant. In other words, the exposure age of Dated Boulders (see study area section below) is the same as the age of the last time that the surface eroded. As the age of the deposits chosen for this research spans three different periods of glaciation, it is likely that the climate underwent some extreme climate changes through time even if all locations experienced the same conditions. Thus temporal changes in my data may also represent changes due to changing climates. The area of northern California where the study is located, is thought to have been both colder and wetter during the glacial periods (Rood et al., 2011). Thus, vegetation also likely changed. Therefore I hypothesize that time periods that include glacial periods would be characterized by faster cracking due to the increased moisture, while drier interglacial periods would be marked by a decrease in cracking rates. It is common knowledge in the geomorphological community that climates that are warmer and wetter undergo more rapid chemical weathering (Shroder 2013). If mechanical weathering follows similar behaviors, then an increase in cracking rates should be seen within the surfaces that experienced glacial events. In times of warmer climates, vapor pressure and humidity would be higher, allowing for more water to be held in the atmosphere, creating an environment where water vapor can easily infiltrate cracks in rock.

## CHAPTER 3: STUDY AREA

Mono Lake is located within the Mono Basin of California, which was formed through the rifting of the Sierra Nevada Mountains in the Basin and Range province over the last five million years. The 45,133 acre lake formed at the base of the Sierra Nevada Mountains around 750,000 years ago, after the Long Valley eruption sequence. The Sierra Nevada Mountains are the result of the uplift of granitic plutons during the Nevada Orogeny in the Mesozoic Era. During the Miocene Epoch, the Basin and Range tectonics produced continental rifts and tilted fault blocks that formed the Sierra Nevada Mountains. This uplift coincided with a global cooling cycle, and glaciers covered the headlands of the field area.

### *3.1. Geomorphology of the Mono Basin*

The study area is located at the outlet of the watershed of 1) the Mill Creek tributary that drains about 1,630-2,070 km<sup>2</sup> of the Eastern Sierra Nevada Mountains, and that flows into Mono Lake (Figure 4), and 2) the Buckeye Creek sub-watershed, that drains 145 km<sup>2</sup> (Figure 5). Both watersheds are underlain by the Cretaceous age Yosemite Valley intrusive suite, which is covered in Pleistocene age glacial deposits (Bailey, 1989). The intrusive suite is composed of granodiorites characterized by 39% plagioclase content, 28% potassium feldspar, 29% quartz, and 5% biotite, and quartz monzonites (Rinehart and Ross, 1964). The granite has undergone minor metamorphic alteration, mostly in the case of biotite to pennite and sphene, and sericitization from the plagioclase.

At the mountain front of both watersheds, there are numerous geomorphic landforms including moraines, outwash terraces, and fluvial terraces formed throughout the Pleistocene and Holocene. Rood (2011) completed extensive geomorphic mapping and dating of these deposits (Figure 6 & 7). The four main glacial events that affected the area, as defined

by Rood (2011) are 1) McGee (2.6-2.0 mya), 2) Sherwin (820 ka), 3) Tahoe (170-130 ka), and 4) Tioga (15-20 ka) (Moore, 2013). Subsequent researchers have included at least one more glacial event; the Mono Basin event (120-109 kya) (Nixon, 2013). Each glacial event left a series of moraines – glacial debris that mark the furthest transgression of the ice – but only a few have been sufficiently preserved in the field area for dates to be taken from them. The oldest moraines in this area would have been overrun by subsequent glacial events that were able to move past the previous finish “line”. In addition to glacial moraines and fluvial outwash terraces, stranded floodplains left behind from the melting of the glaciers are also present in the field area in association with the Tioga, Mono Basin, and Tahoe glaciations (Figure 6).

Moraine crests and outwash terrace surfaces are characterized by granitic rock debris which come in a wide variety of sizes, from gravel to boulders. Rood (2011) determined the exposure age of boulders using  $^{10}\text{Be}$  methods. Table 1 depicts the exposure ages and location data of all boulders used in this study (see methods) that were dated by Rood (2011). The premise behind the  $^{10}\text{Be}$  method is that radionuclides such as beryllium accumulate and decay at a known rate within a rock once it is exposed. By measuring the amount of the nuclides present within a sample, it is possible to back-calculate how long the sample has been exposed at the surface. These “exposure ages” that Rood (2011) calculated for the individual boulders may vary slightly from the “actual age” of the deposition of the sediments associated with moraines they were found on. In this study, however, where I am interested in exposure time, this difference should not impact my results. Here I will use the average *exposure age* of the boulders on a surface, even if the age of the glaciation is much older, with the assumption that the boulder has been stable during its accumulation of  $^{10}\text{Be}$ . Thus, the actual dates being used herein for the exposure age of boulders studied are; 17.10 ka for the Tioga outwash terrace, 45.80 ka for the Mono Basin moraine, and 167.40 ka for the Tahoe outwash terrace. Adjacent to Lundy Canyon and Buckeye Canyons, California (Figure 7), a series of dated outwash terraces and

moraines range in age 13.4 kya to 101.1 kya (Rood et al., 2011). In this area there are 3 main glacial moraine deposits, left behind by glaciers from the Tioga (15-20 ka), Sherwin (820 -730 ka), and Mono Basin (120-109 ka) events. Additionally, there is a dated outwash terrace belonging to the Tioga glacial event (Rood et al., 2011). From these mapped surfaces I selected four surfaces which would provide a range of ages. In addition, based on the field area, I selected two additional surfaces, a Holocene age terrace (I estimate its age as 5 ka), and a modern wash (0 ka), to further flesh out the age range. Table 1 depicts the ages and other miscellaneous information for each different geomorphic surface examined in this study. In the following paragraphs I describe the general geomorphic characteristics of each surface (Figure 8). The **Modern Wash** is located within Mill Creek, and is surrounded by overhanging pines and scrub. This creek maintains low levels during the winter, and becomes more active as snow deposits from the mountains melt. Surface relief is minimal (0.5m), and the area is overhung with pine trees, along with reeds along the border of the stream

The **Holocene Terrace** is located ~15 feet from the banks of the Modern Wash, and extends along the un-forested stream unaffected by any current stream activity. Ground cover consists of dead pine needles from the surrounding tree cover and several small shrubs including common sagebrush. It contains a 3-4 inch deep covering of pine needles from the 3ft in diameter trees found on the surface. The transect in this area is taken along a 75 degree bearing, the boulder bar comprising this site exhibits a surface strike of 133 degrees and a dip of 10 degrees. Overall surface relief is greater than the modern wash at 3.5 meters.

The **Lundy Canyon Tioga Outwash** is covered primarily in sagebrush, and wildflowers, with very few 1ft diameter trees. Only about 7-10% of the ground is free from vegetation and average surface relief is 1.03m. The moraine is split into an upper and lower section by fault activity. The Dated Boulders here are primarily located on the lower section of the moraine. At the Tioga Moraine, in Lundy Canyon, three Dated Boulders are located on this

surface. The moraine is primarily sage and scrub, and the moraine itself is narrow compared to the others in this location. The average surface relief was 10m, with most of the Dated Boulders being located in a small valley within the moraine. The Mono Basin moraine is primarily covered with sagebrush and shrubs, but also contains several 10 inch in diameter trees. The moraine was sandy, with a lower presence of small “boulders” than the previous locations. The average relief of the surface was 2.58m.

The **Tahoe outwash terrace**, located in Buckeye Creek, is covered with sagebrush, and large amounts of wildflowers. Only about forty percent of the ground is free from vegetation. The surface itself is sandy, with a sparse distribution of boulders throughout the entire surface. Average surface relief was 1.39m, though many of the boulders are flush with the ground surface.

The **Sherwin Moraine**, located in Lundy Canyon, is primarily covered in sagebrush and shrubs, alongside stubby (8in in diameter) tree clusters. This moraine is the biggest and oldest of the three moraines observed. The average surface relief is 3.38m. There are barely any smaller boulders, as the surface tends towards medium to large boulders, unlike the other surfaces. The Dated Boulders on this surface are located on the flat top, and side of the moraine. No data for Transect Boulders was collected on this surface, however six Dated Boulders are located here.

Out of these six surfaces, three of them were terminal glacial moraines. Moraines form when glaciers retreat from their original extent, leaving behind a mound of unconsolidated glacial till and erratics. These moraines gain sediment from outwash carried by glacier runoff as the glacier retreats. Even though the moraines were deposited several thousand years ago, the beryllium 10 dates taken for each surface reflect the last time the moraine’s surface was seriously disrupted, via earthquake or landslide for example, exposing clasts to the surface. The surfaces are all within a  $\sim 3 \times 10^{-3} \text{ km}^2$  area, with the exception of the



Tahoe outwash terrace in Buckeye, which was located a 30 minute drive from the original field location, thus their vegetation and climate are likely to have been similar to each other over time, even if the climate has changed during the exposure period. The boulders found on these surfaces would presumably have contained pre-existing cracks prior to their transportation by glacial ice or streams. However, here I assumed that any major fracture would have broken during transportation, such that deposited boulders were relatively uncracked at deposition. The modern wash data will confirm this assumption.

### *3.2. Paleoclimate and Modern Climate*

The paleoclimate of the Mono Lake area has been the subject of much study (Kessler et al., 2006, Anderson, 1990, Bruening et al., 2017, Solomina et al., 2015, Stine, 1989, Bowerman, 2011, Zimmerman, 2011). Commonly, paleoclimate data is inferred using proxies like prehistoric pollen, volcanic ash deposits, and lake sediment cores. Cores taken from the Eastern Sierra Nevada Mountains indicate lowered lake levels during the early Holocene (Anderson, 1990). Data from areas near the Tioga Pass indicates that during the early Holocene (10,000-6,000 ka) there was a lack of enough precipitation to maintain water body levels. Pollen data suggests that many species shifted into higher altitudes around the same time, consistent with drying at lower altitudes. It is thought that during this time, in addition to low precipitation, extremely high summer temperatures, as compared to today, would have been seen. After 6,000 years, precipitation increased, leading to a rise in subalpine conifers and a decrease in the vegetation that occupied any open ground surfaces. In general, glacial advance requires higher precipitation, and lower temperatures. Within the Sierra Nevada Mountains, data collected from rock flour in the Owens River basin indicates that at the very least the Big Pine Creek drainage basin was free from glaciers from 10,000 to 3,200 ka (between the Modern Wash and the Tioga outwash terrace periods), similar to the times put forth by Anderson (1990). If the Big Pine Creek drainage basin was free from glacial activity, there is a

good chance that the Mono Lake field area could have also experienced similar conditions since it is located about an hour south of Mono Lake. Other studies set in Owen's Valley that use rock flour, show that the introduction of rock flour into lake systems is highest during peak glacial periods. These periods could have been controlled through a combination of low insolation and colder temperatures, not just higher precipitation. The lows, or lack of glacial activity, indicated by minimal rock flour accumulation are shown to occur at 64ka, 60 ka, 43 ka, and 36 ka. Simulations for the last glacial maximum in the Sierra Nevada area indicate that a paleoclimate about 5.6°C cooler, with around 200 mm more annual precipitation would have been needed to create the higher equilibrium line altitude that represented the extent of the Tioga glacial advance in the central Sierra Nevada (Kessler et al., 2006). The tree- line would have moved downward towards the scrubland during this period due to glaciation. The modern climate of the study area is characterized by an average yearly maximum temperature of 16.5 degrees Celsius, with the average minimum temperature falling closer to 0 degrees Celsius (Western Regional Climate Center – Mono Lake Station). The Mean Annual Temperature is 47.5 degrees Celsius. Average yearly precipitation for the area is 353.3mm, with most of the precipitation falling in the winter months of November through February as snow. The area contains a large distribution of sagebrush, and closer to the tributaries that flow into Mono Lake, aspens, willows, lupine, desert paintbrush and lodgepole pines are commonly found.

## CHAPTER 4: METHODS

Two different datasets were collected for each of the 5 geomorphic surfaces (Tables 2 & 3) selected for study. In one dataset, I collected data on individual boulders that had been directly dated by Rood (2011) using Beryllium 10 dating. As such, this dataset – hereafter termed Dated Boulders – provides insight into crack behavior on large clasts on rocks that have specific exposure ages. Because all the Dated Boulders are >1m in maximum diameter, I collected a 2<sup>nd</sup> dataset on 5 surfaces, whereby I selected 100 clasts of a range of sizes (see below for details). This second dataset – hereafter referred to as the Transect Boulders with the recognition that some are not actual ‘boulders’ – allows for insight into crack behavior on smaller clasts, that may not be under the same environmental stress as the Dated Boulders. It is important to note that although the rocks in this study are located in the same areas, the data from each of them cannot be analyzed together. The differences in the sizes of the boulders, as well as the dated surfaces they represent are too different to compare within the same graph and would misrepresent the data collected. Due to the location from which the data is being taken from, government land, it is important to note that I did not search for plumose structures on the rocks because doing so would disturb more of the surface than my permit allowed.

### *4.1. Dated Boulder Data Collection*

Dated Boulders were all greater than 1m in diameter in at least one dimension and had been selected by Rood (2011) based on size criteria. Because the coordinates – provided by Rood (2011) to four decimal degrees in NAD27 projection for each boulder were not sufficiently precise to be sure of correct boulder identification in the field, I established an index to quantify confidence that I was collecting measurements on the correct boulder. The first criteria was that the boulder location matched the given coordinates to the fourth decimal

place and was either the only boulder in the area, or the only boulder that fit Rood's (2011) original selection criteria. Next, evidence of sampling was identified by looking for "fresh" loose rock pieces, sampling chisel marks and unusual oxidation or varnish on the boulder (Figure 9). The confidence was then recorded as being low (1): One of many rocks in the area, lack of evidence of previous sampling, does not meet sampling criteria put forth by Rood et al. (2011) to high (4): GPS coordinates match, only rock in the area, evidence of previous sampling such as freshly broken pieces, oxidation varnish, sampling marks, and size meets the sampling criteria. For each boulder I made measurements using a standardized form (Supplement A), and collected the following data:

- 1) The length, width, and height of the boulder were taken with the meter tape.
- 2) Average grain size for the mafic and felsic minerals within the rock, and what minerals were present as a percent.
- 3) Angularity and sphericity of the boulder was quantified as an index value using the standard chart for grain shapes (Figure 10).
- 4) A binary value for whether or not granular disintegration, as evidenced by whether or not loose material on the boulder was present where 0 = no, 1 = yes
- 5) The amount of lichen and/or varnish based off of a 0-4 scale.  
1 representing 0- 30% coverage, 2 representing 30-60% coverage, 3 representing 60-90% coverage, and 4 representing more than 90% coverage.
- 6) The presence of any visible fabric within the boulder, such as foliation or a vein, and its strike and dip or trend and plunge.

Because the Dated Boulders were all large, it was logistically infeasible to count all cracks on their surfaces. Boxes that encompassed representative sections of the boulder were identified instead. This way, the box would allow for a representative quantification of the cracking characteristics of the Dated Boulder, without having to collect data for the entire exposed surface. In order to decide how many representative boxes were needed for the Dated Boulder in question, I developed a set of guidelines. If the boulder was less than 1.5 m long, two boxes were drawn. If the boulder was between 1.5 m and 3m, then three boxes were drawn. Any boulder greater than 3m had four boxes drawn on its surface. In this way, more cracks were measured on larger boulders, thus hopefully providing more accurate representation of any potential spatial variability in cracking across a single boulder. I chose to only locate boxes on upward facing surfaces of the boulder because those surfaces are usually the most stable, as opposed to the sides of a boulder. Each of these measurement areas for all Dated Boulder data – here termed boxes - were 20"x20", and thus were characterized by a surface area of 400 cm<sup>2</sup>. A stencil was employed to mark with chalk the box area.

In order to avoid sampling biases in selection of the location for boxes, I used a selection system based on the boulder size. For example, for a 1.5m long boulder, the maximum width of the boulder was halved and the maximum length divided by three in order to locate the center mark for two boxes. A similar method was used but with fewer or more divisions for the smaller and larger boulders respectively. (Figure 11). For each representative box, the characteristics mentioned above were recorded, with the addition of data regarding cracks <2cm within any average square decimeter in the representative box on the boulder. The number cracks could be rated from 0-3, with 0 meaning no micro- cracks, 1 meaning one micro-crack per square decimeter, 2 meaning 1-5 micro-cracks per square decimeter, and 3 meaning 5 or more micro-cracks per square decimeter.

#### *4.2. Transect Boulder Data Collection*

For each geomorphic surface (Table 1), I selected one or more locations for Transect Boulder data collection. The boulder transects on each surface were generally located on center of the highest regions of the surfaces, like boulder bars on terraces, where theoretically it would be the most stable. I looked for areas with sufficient numbers of boulders that clearly were not part of any bedrock.

The nature of the transect locations varied somewhat by surface. Within the creek, I made measurements (see below) on three active, un-vegetated bars. On the Holocene age terrace, I found a single well-expressed boulder bar. For the Tioga outwash site, I located a well-expressed boulder bar towards the toe of the terrace (letter D in Fig. 8). For the Tioga and Mono Basin moraines, the boulder transect was located at the top of the moraine crest, the most stable area. The Tahoe Outwash Terrace near Buckeye Creek required a different approach. In this location, there were no concentrations of boulders anywhere on the surface. Thus, the entire surface was used as a boulder transect, with widely spaced intervals for boulder selection. At each of these locations, 100 Transect Boulders were selected for measurements. Only rocks within a range of 15-50 cm on the long-axis dimension were selected for data collection. This size range was chosen because rocks smaller than 15 cm were more likely to have been disturbed or eroded from larger clasts due to their small size, and it would be too time consuming to look at every single crack on a boulder larger than 50 cm. For each transect location described above, a 30 m tape was laid down, noting the compass direction of the boulder transect. In order to avoid selection bias, the rock closest to each  $\frac{1}{2}$  meter interval on the tape and meeting my size criteria was chosen for data collection (following Aldred et al., 2015). The same data that was recorded for the Dated Boulders was recorded for the Transect Boulders. Representative boxes were not used for Transect Boulders because they were small enough to allow for a total inspection and measurement of all cracks

within a reasonable time frame. For the Transect Boulders I noted embeddedness as an index (Figure 12A). For each Transect Boulder, I measured the dimensions (length, width, height), roundness and sphericity, “embeddedness”, the number of cracks less than 2 cm, whether or not there was granular disintegration, how much lichen or varnish was present, and what type of foliation was present, if any at all.

#### *4.3. Crack Measurements – Dated Boulders and Transect Boulders*

Within each box on every Dated Boulder, and for every visible crack on each Transect Boulder – no boulders were disturbed - every crack (planar void) larger than 2 cm was counted and its characteristics recorded on the crack data sheet (Appendix A) following Aldred (2015). Measurements taken were:

- **Crack Length:** The surface exposure of the length of the crack within the box (or visible on a Transect Boulder) was measured using seamstress tape in centimeters. If there was topography on the rock surface that the crack followed, the tape was laid onto the rock surface and the ‘length’ was measured as the entire surface exposure length of the crack. Seamstress tape was used because of its flexibility and ability to conform to the shape of the crack. For Dated Boulders, if the crack length continued outside of the representative box, the entirety of the crack was then also measured, again using the flexible seamstress tape, but the length of the crack within the box was also noted.
- **Crack width:** Digital calipers were used to measure the portion of the crack with the maximum void space perpendicular to the crack’s length. If the maximum width of the crack was less than what the digital calipers could measure, a crack width comparator was then used to determine the width.

- **Crack relationship to Boulder Features:** I made note of what boulder features, if any, the crack was parallel to: Surface, Foliation, or Longitudinal axis.
- **Sheet Height:** If a crack was surface-parallel, I measured the sheet height. The sheet height refers to the height of the portion of rock separated from the main boulder by a surface parallel crack. The sheet height of the crack was taken as the maximum representative height of the sheet measured with the tail of the digital caliper and reported in millimeters.
- **Micro-cracks:** Due to the high frequency of cracks smaller than 2cm, a categorization system was developed to distinguish micro crack amounts. There were three categories: none, few (<5 per dm), many (>5 per dm), and were based on the presence and frequency of micro cracks within any given 10x10 centimeter area on the rock for Transect Boulders or within the box for Dated Boulders.
- **Crack Orientation:** The strike and dip of the crack, taken using a Brunton compass. If the dip direction was unclear to the naked eye, a drop of water was deployed on a board held parallel to the crack to show what direction the crack was dipping in. All strike measurements were collected using right hand rule.
- **Weathering Index:** A visual index to quantify the degree of weathering of each crack edge was employed (Figure 12B) – that is to what extent the crack edge appeared ‘fresh’ and sharp vs. rounded by exposure. A “1” on the scale indicated that the crack was fresh, with evidence of recent rupture such as flakes or broken pieces. A “2” indicated that the edges of



the crack were sharp, with no rounded edges. A “3” indicated a crack with mostly sharp, but occasional round edges. A “4” on the scale indicated a crack with mostly rounded, but occasionally sharp edges. A “5” on the scale meant that the edges of the crack were all rounded, indicating that the crack was relatively old.

#### 4.4. Crack Density Calculation

Density of the cracks on both the age Dated Boulders and the Transect Boulders was calculated by summing the length of all cracks found on a boulder or within a box, divided by the exposed surface area of rock, which was calculated using a spherical cap equation (Formula 2) for the Modern Wash boulders because of their overall roundness, and the rectangular prism area equation (Formula 3) for the other five surfaces (see below), or simple area for the Dated Boulder boxes. In formula 2; the variables a, b and c refer to the three different axis of the rock, or put simply, the length, width, and height. In formula 3, w= width, h=height, and l=length. A rectangular prism formula was employed on most surfaces for Transect Boulders because most boulders on these surfaces more approximated a cubic form than a spherical form.

$$\text{Formula 2: } 4 \left( \frac{(ab)^{1.6} + (ac)^{1.6} + (bc)^{1.6}}{3} \right)^{1.6} \quad \text{Formula 3: } A = 2(wl + hl + wh)$$

#### 4.5. Thin Section Analysis

Fifteen samples from the Dated Boulders were collected and brought back to North Carolina for petrographic analysis, which would provide insight into the mineral composition of the Dated Boulders (Table 4,5 Supplement E). Each sample was collected

from the top surface of the boulder, away from the edge of the boulder surface. All collected samples were thicker than four centimeters, and larger than the fist (4 cm). I also attempted to select sample spots on the boulders that were set away from the edge of the rock, as well as spots that were not at extreme angles. Portions of the sampled boulders that were already loose were prioritized because I did not want new cracks to form via striking the rock to get a sample. Samples that were not naturally fully separated from the boulder were extracted using a chisel and mallet after receiving a sampling permit from the California Parks Service. Before physically removing the sample from the host rock, north arrows, horizontal lines and the rock sample ID were marked (Supplement E). Appropriate surfaces for slide making were determined by locating a flat surface on the sample large enough to make a ~26mm by 46 mm thin section slide. Slide billets were cut with prepared faces parallel to the natural outer surface of the rock, resulting in a billet 1.5 centimeters tall and roughly the size of a standard microscope slide (2x3 cm). Billets were sent to National Petrographic Service to be mounted and impregnated with epoxy, equivalent to “Epicure” epoxy by Buehler, an industry standard. A mineral percentage count of quartz, feldspar, biotite, and sausseritized minerals (hornblende, chlorite, epidote, sphene), was conducted under cross polarized light, using 600 points per slide (Table 5, Supplement F).

## CHAPTER 5: RESULTS

### *5.1. Rock and Crack Characteristics by Exposure Age*

#### *Transect Boulders*

##### *Modern Wash - 0 ka:*

The rocks on this surface tended to fall between the range of 15-30 cm, with few if any cracks. The presence of micro-cracks also tended towards “few”. There was little to no grus formation, but the presence of varnish on the rocks was high (Table 6). The majority of the rocks on this surface were medium grained granites. Additionally, most of the rocks in the Modern Wash were categorized between 0 and 2 on the embeddedness scale (Table 7). The average exposed area of a rock in this location was 800 cm<sup>2</sup>, with an average length and width of 2.7cm and 11 cm respectively. (Table 3). Of the cracks that were recorded, most of them were small (less than 5.5 cm) and highly weathered due to their location in an active streambed. The average length of a crack for Transect Boulders on the Modern Wash was 35 mm and the average width, 0.3 mm (Table 3). The boulders within this transect had an average crack density of 0.01 mm<sup>-1</sup>, with a total of only 21 cracks found on all 100 boulders. For surface parallel cracks, the average sheet height was 8 mm. Overall, the weathering index of the cracks on this surface was a 4, meaning they were mostly rounded, with an occasional sharp edge.

##### *Holocene Terrace - 5 ka:*

The rocks on this surface were larger than the rocks in the Modern Wash, and exhibited a higher density of cracks. The Holocene Terrace boulders exhibited a high degree of micro- cracks, primarily falling in the “common” to “many” range. The embeddedness of the rocks on this surface was on average 3, indicating that they were more inset than the Modern

Wash. The average area of a rock in this area was  $945 \text{ cm}^3$ , with an average length and width of 35 cm and 11 cm respectively. There are only five instances of grus formation out of the 100 rocks sampled in this location, and there is an equally low presence of lichen and varnish on the rocks along the transect. The average length of a crack for this boulder transect was 86mm, with average widths of 7 mm (Table 3). The boulders on this transect had an average density of  $0.05 \text{ mm}^{-1}$ , with a total of 60 cracks found on all 100 boulders. For the surface parallel cracks that were observed, the average sheet height was 5 mm. Overall, the weathering index of the cracks on this surface was a 3.5, meaning that they fell between having sharp and round edges.

*Lundy Canyon Tioga Outwash Terrace - 17.1 ka:*

The boulders in this area exhibited more evidence of active granular disintegration than younger surfaces, and exhibited higher percentages of varnish cover (Table 6). Micro- cracks on this surface were categorized as common to many, meaning that there were usually more than five cracks per decimeter on the boulders. The typical embeddedness for the rocks on this surface is between 2 and 3, meaning that they were more inset than previous surfaces. The average area of a rock on this terrace was  $975.52 \text{ cm}^3$ , with an average length and width of 29 cm and 11 cm respectively. On this surface, the average crack length for a Transect Boulder was 59 mm, with an average width of 1 mm. The average crack density for the boulders on this surface was  $0.03 \text{ mm}^{-1}$ , observed from 100 boulders. Any surface parallel cracks observed had an average associated sheet height of 4 mm. Overall, the cracks exhibited a weathering index of 2.9, meaning they were mostly sharp with the occasional rounded edge.

*Buckeye Creek Tahoe Outwash Terrace - 45.8 ka:*

The average area of a rock on this moraine was  $735 \text{ cm}^3$ , with an average length and width of 30 cm and 9 cm respectively (Table 3). Roughly ten percent of the Transect Boulders exhibited grusification, and several chlorite veins were observed on the Transect

Boulders. The amount of lichen was minimal, with more varnish occupying the boulders. The micro-cracks on this surface fall into the “many” category, meaning that there were usually more than five micro-cracks per decimeter on the Transect Boulders here. The average crack on this surface had a length of 56 mm, and a width of 3 mm. The average crack density for this surface was  $0.02 \text{ mm}^{-1}$ , with a total of 21 cracks observed over 100 rocks. For surface parallel cracks, the average sheet height was 8 mm. The cracks on this surface exhibited, on average, a weathering index of 3.3, meaning that they were mostly sharp with occasional rounded edges.

#### *Dated Boulders*

##### *Lundy Canyon Tioga Outwash Terrace - 17.1.ka:*

Six of the Dated Boulders were located on this surface, with three on the upper section and three on the lower section (see details in Field Site section). Data was only recorded for five of the boulders dated by Rood (2011) due to an infestation of biting red ants on the last boulder. The average area of a Dated Boulder on this surface was  $549772 \text{ cm}^3$ , with an average length, width, and height of 256 cm, 184 cm, and 95 cm respectively. No Dated Boulders on this surface exhibited granular disintegration and were found to primarily have less than 30% lichen and varnish cover. The strikes of the representative boxes vary, with the smallest strike being 13 degrees and the largest being 343 degrees. The average strike of the representative boxes was 203 degrees. Micro-cracks on the Dated Boulders on the surface were categorized as mostly “common” meaning they had between one and five micro-cracks per decimeter. For the Dated Boulders on this surface, the average crack length was 116 mm, and the average crack width was 10 mm. The average crack density between the five Dated Boulders was  $0.15 \text{ mm}^{-1}$ , with a total of only 17 cracks being observed across the entire surface. For these 17 cracks, the average weathering index reported was mostly rounded with

the occasional sharp edge. The average sheet height for the cracks that were surface parallel was 4 mm. The ratio of the mafic mineral biotite, to the felsic minerals of quartz and feldspar ranges from 0% to 0.07% in the rocks on this surface.

*Lundy Canyon Tioga Moraine - 14.9-20.7 ka*

Only three of the six boulders dated by Rood (2011) were found and confidently identified on this surface. The average area for a Dated Boulder on this surface was 100,420 cm<sup>3</sup>, with average lengths, widths, and heights of 134 cm, 99 cm, and 77 cm. These boulders did not exhibit any granular disintegration, and only had two instances of lichen or varnish coverage greater than 60%. The strikes of the representative boxes were relatively close in values, with the smallest strike being 54 degrees and the largest being 354 degrees. The average strike of the representative boxes was 222 degrees. Micro-cracks on the Dated Boulders on the surface were categorized as mostly “common” meaning they had between one and five microcracks per decimeter. For the three Dated Boulders observed on this surface, the average crack length was 800 mm, with an average width of 77 mm. The average crack density mathematically came out to be 0.08 mm<sup>-1</sup>, however only one (1) crack was observed within the Dated Boulders on this surface. For this singular crack, the weathering index was reported as a 4, meaning mostly rounded edges with the occasional sharp edge. There were no incidences of surface parallel cracking. The ratio of the mafic mineral biotite, to the felsic minerals of quartz and feldspar was 0% in the one sample from this surface that was big enough to turn into a thin section.

*Lundy Canyon Mono Basin Moraine - 45.8 ka:*

There were six Dated Boulders located on this surface, with an average area of 504,708 cm<sup>3</sup>. The average length of the Dated Boulders was 206 cm, the average width was 172 cm, and the average height was 94 cm. Half of the boulders in this area exhibited granular disintegration, with an average amount of lichen and varnish cover of 45%. The

strikes of the representative boxes vary a decent amount, with the smallest strike being 11 degrees and the largest being 359 degrees. The average strike of the representative boxes was 161 degrees. Micro-cracks on the Dated Boulders on the surface were categorized as mostly “common” meaning they had between one and five micro-cracks per decimeter. With the data taken from all six Dated Boulders on this surface, the average crack was calculated to have a length of 132 mm, and a width of 5 mm. For this surface, the average crack density was  $0.22 \text{ mm}^{-1}$ , with a total of 21 cracks being observed. Some of these cracks were surface parallel and had an average sheet height of 7 mm. Overall, the 21 cracks had an average weathering index of 3.3, meaning that they were mostly sharp with occasional rounded edges. The ratio of the mafic mineral biotite, to the felsic minerals of quartz and feldspar ranges from 0% to 0.04% in the rocks on this surface.

*Buckeye Creek Tahoe Outwash Terrace - 167.4 ka:*

There were eight Dated Boulders located on the Tahoe outwash terrace, with an average area between them of  $421,359 \text{ cm}^3$ . The average length of a Dated Boulder here was 193cm, the average width being 115 cm, and the average height being 61 cm. Almost all of the boulders on this surface exhibited granular disintegration. Only one boulder out of the eight had a 90% coverage of lichen, the rest had between 0 and 30% lichen and varnish cover. The strikes of the representative boxes vary less than the Mono Basin Moraine, with the smallest strike being 4 degrees and the largest being 335 degrees. The average strike of the representative boxes was 155 degrees. Micro-cracks on the Dated Boulders on the surface were categorized as mostly “many” meaning they had more than five micro-cracks per decimeter. The average crack on the Dated Boulders of this surface had a length of 60 mm, and a width of 1 mm. The average crack density for the boulders on this surface was  $0.01 \text{ mm}^{-1}$  with only 13 cracks being observed over 100 rocks. For these 13 cracks, the average

weathering index was 3.6, meaning that they tended towards being rounded, with the occasional sharp edge. The frequency of boulders on this surface was less than the younger surfaces before it. On this surface, the average crack had a length of 193 mm, and a width of 1 mm. The average density of cracks for the eight boulders located at Buckeye Creek was  $0.16 \text{ mm}^{-1}$ , with 18 cracks being identified. For the surface parallel cracks, the average sheet height was 7 mm. Overall the cracks on this surface exhibited an average weathering index of 3.3, meaning that they were mostly sharp with the occasional rounded edge. The ratio of the mafic mineral biotite, to the felsic minerals of quartz and feldspar ranges from 0% to 0.03% in the rocks on this surface.

*Lundy Canyon Sherwin Moraine - 45.6-133.6 ka:*

There were six Dated Boulders on this moraine, with an average area of  $216,589 \text{ cm}^3$ . The average length of a Dated Boulder was 142 cm, the average width was 98 cm, and the average height was 80 cm. Similar to the Dated Boulders on the Mono Basin moraine, half of these boulders exhibited granular disintegration. Only one boulder had lichen coverage greater than 90%, all the rest had coverage of both lichen and varnish between 30% and 60%. The strikes of the representative boxes vary greatly, with the smallest strike being 26 degrees and the largest being 354 degrees. The average strike of the representative boxes was 191 degrees. Micro-cracks on the Dated Boulders on the surface were categorized as mostly “many” meaning they had more than five micro-cracks per decimeter. The average crack length and width between the six Dated Boulders located on this surface was 61 mm and 6 mm respectively. There were no surface parallel cracks observed. The average density of cracks between the six boulders was  $0.12 \text{ mm}^{-1}$ , spread over 13 boulders. The average crack on this surface had a weathering index value of 3.7, meaning that they were mostly rounded with the occasional sharp edge.



## 5.2. Chronofunctions of Rock and Crack Data

In the following sections, I present time trends – chronofunctions - for different properties of the rocks from which measurements were made and for the cracks themselves.

### *Rock Properties*

*Size* – The dimensions of both different types of boulders across the surfaces follows a distinct pattern (Figures 13 & 14). The boulders are largest in the Holocene (5ka) and the Tioga Outwash Terrace (17.1ka), followed by a decrease in width and height as the surfaces get older (Figures 13 & 14). The smallest Transect Boulders were found on the Mono Basin moraine, with the largest located on the Tioga outwash terrace. The surface area of boulders decreased over time as well, with boulders with higher surface areas being found on the Holocene and Tioga Outwash Terraces. On older surfaces, the surface area decreased.

*Shape* - The changes in sphericity and angularity of both boulder types show an overall pattern of decreasing angularity, and increasing sphericity as the surfaces get older (Figure 15). The majority of Transect Boulders of all ages exhibited a sphericity of S3, however, the S4 designation was a close second. The angularity measurement was found to be R3 for the Transect boulders, although the number of Transect Boulders with angularity of R4 was almost as high.

*Coatings* – When considering the presence of lichen and varnish on the boulders in the area, there does not appear to be a consistent change in lichen coverage through time other than the initial establishment of lichen between

‘zero’ time and the Holocene (Table 6; Figure 16). With the exception of the Modern Wash, all boulders on the surface exhibited between 0 and 30% lichen coverage, with none exceeding 30%. A similar result was found when looking at coverage patterns of varnish across the seven surfaces (Figure 16 A). However, looking at the count of instances of coverage for each surface boulder, a pattern begins to emerge (Figure 16 B). Just looking at the surfaces on which transects were counted, an increase in the number of boulders with lichen and varnish coverage from the Holocene Terrace into the Tioga Outwash Terrace, can be seen. The instances for Mono Basin Moraine, and Tahoe Outwash show a decrease from the maximum count on the Tioga Outwash Terrace.

*Embeddedness* - The embeddedness of a boulder has a direct correlation to the surface area exposed to mechanical weathering, an embeddedness of 4 means that there is less surface area exposed than for a rock with an embeddedness of 1. Embeddedness varies somewhat with age, with overall higher embeddedness on the Holocene Terrace (5 ka) and lowest on the Modern Wash (0ka). Embeddedness is deepest at the Holocene Terrace (5 ka), with 89 clasts falling into category 3, and Buckeye Terrace (40ka), with 71 clasts falling into category 3. (Figure 16A, Table 7)

*Misc. Boulder Properties* – Granular disintegration increases in Transect Boulders over time, as well as the number of cracks smaller than 2 cm (Table 9 &10).

#### *Crack Properties*

*Length* - The lengths of cracks on boulder transect clasts starts off relatively short (35 mm average) within the Modern Wash, but increases in the Holocene Terrace (86 mm average; Fig. 16 &17). Rocks on older surfaces

experience an immediate decline in crack length after about 5 ka years, followed by a slower decrease in crack length as the surfaces get older. (Figure 17 & 18).

*Width* - The widths of cracks peak at 5 ka, and decreases steadily from there. (Figures 17 & 18). Overall, after 5 ka, the crack widths on boulder transects show an inverse relationship between crack width and the age of the surface, with boulders on older surfaces having thinner cracks, with average width decreasing from 6.9 mm on the Holocene (5 ka) surface to 1.19 mm on the Tahoe Outwash surface (84 ka).

*Density* - The density of cracks within the boulder transects is initially low on boulders found in the modern wash ( $0.008 \text{ mm}^{-1}$  on average), but then increases to  $0.018 \text{ mm}^{-1}$  on the Holocene Terrace boulders. After the Holocene Terrace, the crack density decreases again as older surfaces have lower density of cracks (Figures 19 & 20).

*Type of cracks* - There were five different categories of cracks recorded from the clasts: surface parallel, longitudinal, through- going, fabric and “other”- where the cracks were not a specific type- (Table 8). Surface parallel cracks were most common in the Holocene and Tioga Outwash terraces, and decreased steadily as the surface got older (Figure 21). The most through-going cracks were found on the Holocene Terrace, once again decreasing in quantity on the older surfaces. Longitudinal cracks were most plentiful on the Tioga Outwash Terrace, and decreased in number on all the older surfaces. There were not as many instances of fabric cracks as the other four types of cracks, but the Tioga Outwash Terrace contained the few that were collected. The last type of crack, “other”, had a similar pattern to the surface parallel

cracks, with most of them being present on the Holocene and Tioga Outwash terraces.

### *Orientation*

*Strike-* The overall strike of the cracks from the Dated Boulder dataset is on a Northeast/Southwest strike line, while the overall strike for the Transect Boulders is split between Northeast, and Northwest. As the ages of the surfaces increase, the strikes move from North-Northeast, to North-Northwest (Figure 22, 23). Only on the very oldest surface, the Sherwin Moraine, does the strike come back to a North- Northeast direction.

*Dip* – In past work, crack orientation dip angles generally fall between 45 and 90 degrees (Eppes, 2015). The dip angles from this particular study follow the same pattern, with the values ranging from 13 degrees all the way up to 88 degrees across all surfaces. It appears that average dip angle slightly increases over time, from 45 degrees on the Modern Wash, to 55 degrees on the Mono Basin Moraine. The dip angle does decrease again on the Tahoe Outwash Terrace, back down to 46 degrees (Figures 24 & 25).

## CHAPTER 6: DISCUSSION

The data collected in this study are not precisely consistent with my original hypothesis that chronofunctions of mechanical weathering over time would look similar to those for chemical weathering (Figure 1). The chronofunctions presented herein show a rapid growth and accumulation of cracks in the rock early on from exposure, followed by a decrease in visible cracking on the rock, which then remains stable. I interpret apparent 'decreases' in crack length with time as indicating that the cracks are breaking pieces of the rock off from the main body – necessarily removing the crack from the family of cracks on the boulder at its maximum length. This trend is evident for all crack characteristics measured (length, width, and density (Figure 16-20), grusification, and cracks <2cm). I would like to note that these trends are non-linear, even though they appear as linear within the graphs. Due to the large chunk of missing time between the Tioga Moraine and the Tahoe, I did not want to fit curves to a dataset with a gap.

Observed trends in crack size and density can be explained by pieces of large boulders falling off over time, decreasing the overall size of the boulder, and effectively removing what would have been the visible crack on the boulder. For the Transect Boulders, the dimensions of the boulders decrease over time starting with rocks found on the Holocene surface (Figure 14). This idea is supported by the presence of what I termed "daughter boulders", chunks of the identical rock types as the boulder in question, found on the ground within a foot of the original boulder (Figure 27). On the Tahoe Outwash Terrace especially, much of the ground was covered in grus, with many of the boulders measured being almost flush to the ground (Figure 8). Because I know grus is produced via the mechanical weathering of rocks, it is also likely that boulder size is reduced through time both by granular disintegration and erosion, but also by being buried in their own debris as they are being

weathered. The boulders in the field area did not show a significant relationship between grusification and age (Table 10) supporting the idea that it is an ongoing process that begins immediately upon the exposure of the boulder and continues through time – as opposed to the through-going cracking slow-down that I observe. That boulders lose material through time is also supported by the shapes of the clasts through time as they change from less spherical/more angular to more spherical with rounded edges (Figure 15D). Maybe this is speaking to the early dominance of through-going cracking – that leaves behind angular pieces, followed by dominance of grusification that rounds corners. Mechanical stresses tend to be highest on corners, which concentrate the stresses much like flaws (Eppes and Keanini 2017). The presence of lichen and varnish, while noticeable, did not display any useful patterns suggesting they can grow sufficiently quickly to reflect the boulder breakdown over time.

What the data suggests is that after the initial deposition of the clast on the surface, crack growth is initially fast. In other words, any crack that was under enough stress to propagate, and had the room to do so, and quickly. After that crack split the rock and was removed, however, remaining smaller cracks must not experience significant enough stresses to force them around a mineral or obstacle blocking their progress. These data suggest, then, that for boulders on the order of  $<1$  m in size, there is a limited population of cracks that are highly susceptible to ‘normal’ environmental stresses. Another interpretation could lie in the addition of chemical weathering after exposure, where the growth of rock varnish through chemical weathering leaves behind a resistant coating (case hardening) which does not allow for easy crack propagation, keeping the cracks shorter. The types of crack appear to change over time, from surface parallel to through-going cracks (Figure 20). This could be due to initial weathering occurring at weak spots on clasts, primarily along surface planes and corners. I infer that once these pieces are weathered enough, the clast no longer has primary features

that stresses can concentrate on, leaving the unspecified cracks behind, which, if they lack sufficient stress, will not continue to propagate any further.

Crack orientation can be seen to change through time; however we must be continuously aware that glacial moraines and terraces are not stationary landmasses, but are subject to new geomorphologic activity through time. What could be happening is that the clasts that the data was collected from, may have had pre-existing weaknesses from their time in bedrock, which were carried with them as the clasts were deposited. I believe that the pre-existing weaknesses would get uniformly exploited, creating some of the preferred directions I saw in the field. At the same time however, I also think that it is entirely possible for cracks to develop in random directions according to flaws within their own make-up, not necessarily just due to jointing or the fabric of the rock. Or, after deposition, the clasts were moved through a subsequent geomorphic process such as a later glaciation. Thus, one would hope that clast orientations within their respective surfaces would be similar, there is no guarantee that this is the case.

A similar study was conducted by D'Arcy et al, in 2014, in the Lone Pine area of California, south of Mono Lake. The clasts the D'Arcy collected data on were all granitic and ranged from 0.5m to 3m in size. His data focused on measuring fracture width in these clasts and showed an increase in fracture width with a surface's age. His research also involved measuring the orientations of the fractures, which he displayed in rose diagrams according to glacial and interglacial periods. For the interglacial periods, the data shows a single preferential orientation of N/S. For the glacial periods, two preferential orientations were observed, one from NE/SW, and another from NW/SE. These orientations are almost the same as those collected from clasts in the Mono Lake and Buckeye locations. What differs between the two sets of data is the width of the fractures, or cracks, within the measured clasts. While according to D'Arcy, the width of the fracture increased with age, the data from

the 2019 field site when all cracks are included – not just the largest rock- splitting cracks as was the case with D’Arcy (2014) - shows a different trend. The data collected shows an increase in fracture width from the Modern Wash (0ka) to the Holocene Terrace (5ka), followed by a continuous decrease in fracture width as the surfaces get older.

The length of cracks increase suddenly around the 5 ka mark, then rapidly, and continuously decline as the surfaces get older (Figure 16,17). This possibly could be due to the crack reaching a terminal length within the boulder as it ages, and then bisecting the boulder, so that a piece of the rock falls off, removing the crack entirely. This would certainly remove any sizable cracks on older surfaces, and just leave behind the smaller cracks that could not propagate.

A similar reasoning could be behind why older surfaces appear to have thinner cracks. Cracks that are wider probably have more stress concentrated at their tips, therefore can propagate easier. Once they fully propagate across the surface of the rock, the chunk containing the crack falls off, leaving behind a fresh surface, where cracks need to start anew. This action happening repeatedly over thousands of years would leave an older rock with only the small, thin cracks that never made it to the edge of the boulder. The density of cracks once again is highest around 5 ka, during the Holocene, and the density decreases as the surfaces get older. Possibly due to the removal of major cracks through time, leaving behind smaller cracks. Most of the crack orientations trend in the same direction, and for those that do not, re- excavation and movement from subsequent glacial activity or landslides could have moved the boulders around from their original position, changing the orientation of the cracks.



## CHAPTER 7: CONCLUSIONS

Mechanical weathering in boulders found on the eastern margins of the Sierra Nevada mountains show trends in time whereby 1) total crack length increases then decreases over time, 2) crack density also increases then decreases over time, 3) the dominant type of crack changes over time, from surface-parallel cracks, to through-going cracks and 4) this temporal behavior of mechanical weathering is similar overall to that of chemical weathering.

These observations are overall supportive of my original hypothesis, rocks would have experienced a sharp increase in crack activity, and as time moved on, the crack activity would plateau. However, in this original model, I did not predict the decrease in the crack size and density that would naturally occur as cracks propagate fully through and essentially ‘disappear’. Regardless, the data presented documents a previously unknown pattern of activity for mechanical weathering. What is interesting is that this pattern is almost identical to the behavior of chemical weathering in nature, showing a link between the two major weathering classes.

While this result may seem to be obvious, this is one of the first field- datasets to document this evolution. Even though mechanical weathering plays a large role in the evolution of earth surfaces, geologists have taken it for granted that rates of mechanical weathering are linear over time. One of the most common types of age dating for rocks,  $^{10}\text{Be}$  dating had been operating on the assumption that mechanical weathering happens at this consistent – linear - rate. As seen in this study, that is not exactly the case. Thus, there needs to be an understanding of this possibility when interpreting  $^{10}\text{Be}$  dates. For example, attention could be paid to the paleo and current climate of the field area, in order to have a better idea of what could have happened to the rocks undergoing the dating process. On a

historical preservation front, this research provides some useful information into whether or not current preservation techniques are actually helping to preserve a monument, versus accelerating rock breakdown. If treatment like walnut-shell blasting does more harm in the long-term, different approaches may need to be taken to ensure preservation.


This research only encompasses one area in a particular climate and can only give insight to cracking behavior in similar locations. Cracking occurs regardless of where rocks are located or what they're used for, so further research should be encouraged.

Research projects already in the works are attempting to look at mechanical weathering across the ocean in Israel and Owens Valley in California, with plenty of locations around North America that would provide important new insights into the topic at hand. This thesis is not meant to become the “be all end all” of crack behaviors, but it should serve as a solid base for geomorphologists to build upon, and I hope that they do. Mechanical weathering is a process geologists are only beginning to unravel and it is a worthwhile subject for the scientific community to take more serious note of.

## REFERENCES

- Aldred, J., and Eppes, M.C., 2015, The influence of solar-induced thermal stresses on the mechanical weathering of rocks in humid mid-latitudes: *Earth Surface Processes and Landforms*, v. 41, p. 603–614, doi: 10.1002/esp.3849.
- Amit, R., and Gerson, R., 1993, Stages and rate of the gravel shattering process by salts in desert Reg soils: *Geoderma*, v. 57, p. 295–324, doi: 10.1016/0016-061(93)90011-9.
- Anderson, S. R., 1990: Holocene forest development and paleoclimates within the central Sierra Nevada, California. *Journal of Ecology*, 78: 470– 489.
- Anderson, S. P. (2005). Glaciers show direct linkage between erosion rate and chemical weathering fluxes. *Geomorphology*, 67(1-2), 147-157.
- Atkinson, B. K. (1984). Subcritical crack growth in geological materials. *Journal of Geophysical Research: Solid Earth*, 89(B6), 4077-4114.
- Atkinson, B. K., & Meredith, P. G. (1987). The theory of subcritical crack growth with applications to minerals and rocks. *Fracture mechanics of rock*, 2, 111-166.
- Bailey, R. A. (1989). Geologic map of Long Valley caldera. *Mono-Inyo Craters volcanic chain, and vicinity, eastern California: US Geological Survey Miscellaneous Investigations Map I-1933, scale, 1(62,500)*, 11.
- Birkeland, P.W., and Burke, R.M., 1988, Soil Catena Chronosequences on Eastern Sierra Nevada Moraines, California, U.S.A.: *Arctic and Alpine Research*, v. 20, p. 473, doi: 10.2307/1551345.
- Bost, M., and Pouya, A., 2016, Stress generated by the freeze–thaw process in open cracks of rock walls: empirical model for tight limestone: *Bulletin of Engineering Geology and the Environment*, v. 76, p. 1491–1505, doi: 10.1007/s10064-016-0955-

6.

- Bowerman, N. D., & Clark, D. H. (2011). Holocene glaciation of the central Sierra Nevada, California. *Quaternary Science Reviews*, 30(9-10), 1067-1085.
- Brantut, N., Heap, M. J., Baud, P., & Meredith, P. G. (2014). Mechanisms of time  dependent deformation in porous limestone. *Journal of Geophysical Research: Solid Earth*, 119(7), 5444-5463.
- Chen, G., Chenevert, M. E., Sharma, M. M., & Yu, M. (2003). A study of wellbore stability in shales including poroelastic, chemical, and thermal effects. *Journal of Petroleum Science and Engineering*, 38(3-4), 167-176.
- Collins, B.D., Stock, G.M., and Eppes, M.-C., 2018, Thermal influences on spontaneous rock dome exfoliation: Nature Communications, v. 9, doi: 10.1038/s41467-017-02728- 1.
- Cui, K., Wu, G., Wang, X., and Chen, W., 2017, Behaviour of slate following freeze–thaw and dry– wet weathering processes: Quarterly Journal of Engineering Geology and Hydrogeology, v. 50, p. 117–125, doi: 10.1144/qjegh2016-093.
- Eppes, M.C., Bierma, R., Vinson, D., and Pazzaglia, F., 2008, A soil chronosequence study of the Reno valley, Italy: Insights into the relative role of climate versus anthropogenic forcing on hillslope processes during the mid-Holocene: Geoderma, v. 147, p. 97–107, doi: 10.1016/j.geoderma.2008.07.011.
- Eppes, M.C., and Mcfadden, L.D., 2010, Cracks in desert pavement rocks: Further insights into mechanical weathering by directional insolation: Geomorphology, v. 123, p. 97–108, doi: 10.1016/j.geomorph.2010.07.003.
- Eppes, M.C., Magi, B., and Hallet, B., 2016, Deciphering the role of solar- induced thermal stresses in rock weathering: Geological Society of America Bulletin, v. 128, p. 1315– 1338, doi: 10.1130/b31422.1.

- Eppes, M.-C., and Willis, A., 2015, Cracks in Martian boulders exhibit preferred orientations that point to solar-induced thermal stress: *Nature Communications*, v. 6, doi: 10.1038/ncomms7712.
- Eppes, M.-C., and Keanini, R., 2017, Mechanical weathering and rock erosion by climate-dependent subcritical cracking: *Reviews of Geophysics*, v. 55, p. 470–508, doi: 10.1002/2017rg000557.
- Halsey, D.P., Mitchell, D.J., and Dews, S.J., 1998, Influence of climatically induced cycles in physical weathering: *Quarterly Journal of Engineering Geology and Hydrogeology*, v. 31, p. 359–367, doi: 10.1144/gsl.qjeg.1998.031.p4.09.
- Hancock, G.S., Shobe, C.M., and Eppes, M., 2017, Field Evidence For The Influence Of Weathering On Rock Erodibility And Channel Form In Bedrock Rivers: *Earth Surface Processes and Landforms*, doi: 10.1130/abs/2017am-306421.
- Holbrook, W.S., and Brantley, S.L., 2019, Links between physical and chemical weathering inferred from a 65-m-deep borehole through Earth’s critical zone: *Scientific Reports*, v. 9, doi: 10.1038/s41598-019-40819-9.
- Izumiyama, H., Tsutsumi, D., and Fujita, M., 2012, Effect of Freeze-Thaw Action on Porosity Change and Destruction of Weathered Bedrock in Different Lithology and Development of Destruction Model: *International Journal of Erosion Control Engineering*, v. 5, p. 103– 112, doi: 10.13101/ijece.5.103.
- Jamieson M Bruening et al 2017 *Environ. Res. Lett.* 12 014008
- Jenny, H. (1941). *Factors of soil formation*. McGraw-Hill, New York. *Factors of soil formation. McGraw-Hill, New York.*
- Kessler, M. A., Anderson, R. S., & Stock, G. M. (2006). Modeling topographic and climatic control of east-west asymmetry in Sierra Nevada glacier length during the Last Glacial Maximum. *Journal of Geophysical Research: Earth*

*Surface, 111*(F2).

Kirchner, J.W., and Finkel, R.C., 2001, Mountain erosion over 10 yr, 10 k.y., and 10 m.y. time scales: *Geology*, v. 29, p. 591, doi: 10.1130/0091

7613(2001)029<0591:meoyky>2.0.co;2.

Lambart, S., and Savage, H.M., 2018, Experimental Investigation of the Pressure of Crystallization of Ca(OH)<sub>2</sub>: Implications for the Reactive Cracking Process:

*Geochemistry, Geophysics, Geosystems*, v. 19, p. 3448–3458, doi:

10.1029/2018gc007609.

Layzell, A.L., and Eppes, M.C., 2012, Post-glacial range of variability in the Conejos River Valley, southern Colorado, USA: fluvial response to climate change and

sediment supply: *Earth Surface Processes and Landforms*, v. 37, p. 1189–1202, doi:

10.1002/esp.3253.

Luque, A., and Ruiz-Agudo, E., 2010, Direct observation of microcrack development in marble caused by thermal weathering: *Environmental Earth Sciences*, v. 62, p. 1375–

1386, doi: 10.1007/s12665-010-0624-1.

Mcfadden, L., Eppes, M., Gillespie, A., & Hallet, B. (2005). Physical weathering in arid landscapes due to diurnal variation in the direction of solar heating. *Geological*



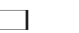
*Society of America Bulletin*, 117(1), 161. doi:10.1130/b25508.1

Meredith, P. G., & Atkinson, B. K. (1985). Fracture toughness and subcritical crack growth during high-temperature tensile deformation of Westerly granite and Black gabbro. *Physics of the Earth and Planetary Interiors*, 39(1), 33-51.

Mingqing You, Strength criterion for rocks under compressive-tensile stresses and its application, *Journal of Rock Mechanics and Geotechnical Engineering*, Volume 7,

Issue 4, 2015, Pages 434- 439, ISSN 1674-7755,

<https://doi.org/10.1016/j.jrmge.2015.05.002>.

- (<http://www.sciencedirect.com/science/article/pii/S1674775515000669>)
- Moore, J.G., and Moring, B.C., 2013, Rangewide glaciation in the Sierra Nevada, California: *Geosphere*, v. 9, p. 1804–1818, doi: 10.1130/ges00891.1.
- Murton, J.B., Peterson, R., and Ozouf, J.-C., 2006, Bedrock Fracture by Ice Segregation in Cold Regions: *Science*, v. 314, p. 1127–1129, doi: 10.1126/science.1132127.
- Murton, J.B., 2016, Monitoring rock freezing and thawing by novel geoelectrical and acoustic techniques: *Journal of Geophysical Research: Earth Surface*, v. 121, p. 2309–2332, doi: 10.1002/2016jf003948.
- Mushkin, A., and Sagy, A., 2014, Measuring the time and scale-dependency of subaerial rock weathering rates over geologic time scales with ground-based lidar: *Geology*, v. 42, p. 1063–1066, doi: 10.1130/g35866.1.
- Nara, Y., et al (2010), Subcritical crack growth and long-term strength in rock and cementitious material, *Int. J. Fract.*, **164**(1), 57-71.
- Nixon, E., 2013, Geologic History of the Mono Basin: [www.indiana.edu](http://www.indiana.edu).
- Ravaji, B., Ali  Lagoa, V., Delbo, M., & Wilkerson, J. W. (2019). Unraveling the Mechanics of Thermal Stress Weathering: Rate  Effects, Size  Effects, and Scaling Laws. *Journal of Geophysical Research: Planets*, **124**(12), 3304-3328.
- Rinehart, C.D., Ross, D.C., and Pakiser, L., 1964, Geology and mineral deposits of the Mount Morrison quadrangle, Sierra Nevada, California, with a section on a gravity study of Long Valley: Professional Paper, doi: 10.3133/pp385.
- Rood, D.H., Burbank, D.W., and Finkel, R.C., 2011, Chronology of glaciations in the Sierra Nevada, California, from <sup>10</sup>Be surface exposure dating: *Quaternary Science Reviews*, v. 30, p. 646–661, doi: 10.1016/j.quascirev.2010.12.001.

- Salvadori, O., & Municchia, A. C. (2016). The Role of Fungi and Lichens in the Biodeterioration of Stone Monuments. *The Open Conference Proceedings Journal*, 7(Suppl M4), 39-54. doi:10.2174/2210289201607020039
- Scarciglia, F., and Pera, E.L., 2005, The interplay of geomorphic processes and soil development in an upland environment, Calabria, South Italy: *Geomorphology*, v. 69, p. 169–190, doi: 10.1016/j.geomorph.2005.01.003.
- Shroder, J. F. (2013). *Treatise on geomorphology*. San Diego: Academic Press.
- Solomina, O. N., Bradley, R. S., Hodgson, D. A., Ivy-Ochs, S., Jomelli, V., Mackintosh, A. N., ... & Young, N. E. (2015). Holocene glacier fluctuations. *Quaternary Science Reviews*, 111, 9-34.
- Sousa, L., Siegesmund, S., and Wedekind, W., 2018, Salt weathering in granitoids: an overview on the controlling factors: *Environmental Earth Sciences*, v. 77, doi: 10.1007/s12665-018-7669-y.
- Stine, S. (1990). Late holocene fluctuations of Mono Lake, eastern California. *Palaeogeography, Palaeoclimatology, Palaeoecology*, 78(3-4), 333-381.
- Valentine, G.A., and Groves, K.R., 1996, Entrainment of Country Rock during Basaltic Eruptions of the Lucero Volcanic Field, New Mexico: *The Journal of Geology*, v. 104, p. 71– 90, doi: 10.1086/629802.
- Vlahou, I., and Worster, M.G., 2015, Freeze fracturing of elastic porous media: a mathematical model: *Proceedings of the Royal Society A: Mathematical, Physical and Engineering Sciences*, v. 471, p. 20140741– 20140741, doi: 10.1098/rspa.2014.0741.
- Walder, J, Bernard, H; A theoretical model of the fracture of rock during freezing. *GSA Bulletin*; 96 (3): 336–346. doi: <https://doi.org/10.1130/0016->



7606(1985)96<336:ATMOTF>2.0.CO;2

Wang, H.F., 1989, Thermal Stress Cracking in Granite: Journal of Geophysical Research, v. 94, p.1745–1758.

You, M., 2015, Strength criterion for rocks under compressive-tensile stresses and its application: Journal of Rock Mechanics and Geotechnical Engineering, v. 7, p. 434–439, doi: 10.1016/j.jrmge.2015.05.002.

Zimmerman, S. R., Pearl, C., Hemming, S. R., Tamulonis, K., Hemming, N. G., & Searle, S.Y. (2011). Freshwater control of ice-rafted debris in the last glacial period at Mono Lake, California, USA. *Quaternary Research*, 76(2), 264-271.

Table 1: Summary Table of basic surface characteristics for all seven surfaces; Age of boulders on each surface taken from Rood (2011). No data was recorded for the Modern Wash and the Holocene Terrace because there were no Dated Boulders located on these surfaces, as they were added by Berberich for the purpose of this research.

\*this surface is an estimated age based on soil development and inset relationship

Surface	Surface ID	Average Age (ka)	Deposit Type	Overall Relief (m)	Overall Slope	Vegetation Types	# of Dated Boulders (DB)	# of Transect Boulders (BT)
Modern Wash	MW	0	River Wash	N/A	N/A	Moss	0	100
Holocene Terrace	H1DB	500	Terrace	N/A	N/A	Pine Trees, small bushes	0	100
Lundy Canyon Outwash Terrace	LCTIO	39617	Outwash Terrace	1.24	2	Sage Scrubland/grassland	5	100
Lundy Canyon Moraine	LCTI	18533	Glacial Moraine	10	24	Sage scrubland	3	0
Mono Basin Moraine	LCMB	39617	Glacial Moraine	2.58	5	Sage scrubland, grassland, wildflowers, Pine Trees	6	100
Buckeye Creek Outwash Terrace	BCTA	226900	Outwash Terrace	1.33	2	Sage Scrubland/wildflowers	9	100
Sherwin Moraine	LCSH	76640	Glacial Moraine	3	18	Sage Scrubland/wildflowers	6	0

Table 2: Summary table of Dated Boulder and Dated Boulder crack characteristics. Crack Length is the average length of all cracks measured in all Dated Boulders. Crack Width is the average width of all cracks measured in all Dated Boulders. Sheet height is the average height of the sheet being dislodged by the surface-parallel crack, measured from all Dated Boulders. Crack Density calculated from the number of cracks on the rock divided by the surface area, then the average was taken from all the Dated Boulders.

Surface	Modern Wash	Holocene Terrace	Lundy Canyon Outwash Terrace	Lundy Canyon Moraine	Mono Basin Moraine	Buckeye Creek Outwash Terrace	Sherwin Moraine
Surface ID	MW	H1DB	LCTIO	LCTI	LCMB	BCTA	LCSH
# of Dated Boulders (DB)	0	0	5	4	6	9	6
Average Surface Area cm <sup>3</sup>	N/A	N/A	192231	45684	154337	92657	63186
Average Rock Length cm	N/A	N/A	246.8	133.7	206.8	193.4	130.5
Average Rock Width cm	N/A	N/A	187.8	99.0	169.6	115.0	83.3
Average Rock Height cm	N/A	N/A	27.4	76.7	87.2	57.5	72.8
Average Crack Length mm	N/A	N/A	121.5	800.0	111.9	193.3	63.0
Average Crack Width mm	N/A	N/A	10.5	77.4	4.0	14.9	2.4
Average Sheet height mm	N/A	N/A	4.0	N/A	7.0	7.4	N/A
Average Crack Density	N/A	N/A	0.0025	0.0013	0.0007	0.0285	0.0008
Average Sphericity	N/A	N/A	3.2	3.3	3.5	2.4	3.4
Average Angularity	N/A	N/A	3.2	2.7	2.7	2.4	3.0

Table 2 continued: Summary table of Dated Boulder and Dated Boulder crack characteristics. Crack Length is the average length of all cracks measured in all Dated Boulders. Crack Width is the average width of all cracks measured in all Dated Boulders.

Sheet height is the average height of the sheet being dislodged by the surface-parallel crack, measured from all Dated Boulders. Crack Density calculated from the number of cracks on the rock divided by the surface area, then the average was taken from all the Dated Boulders.

Average Weathering Index	N/A	N/A	3.5	4.0	3.4	3.3	3.8
Number of cracks	N/A	N/A	15	1	18	18	10
Primary Type of Crack	N/A	N/A	Surface Parallel	Longitudinal	Un-Oriented	Un-Oriented	Un-Oriented

Table 3: Summary table of Transect Boulders and Transect Boulder crack characteristics. Crack Length is the average length of all cracks measured in all Transect Boulders. Crack Width is the average width of all cracks measured in all Transect Boulders. Sheet height is the average height of the sheet being dislodged by the surface-parallel, measured from all Transect Boulders. Crack Density calculated from the number of cracks on the rock divided by the surface area, then the average was taken from all the Transect Boulders. Crack Strike is the vector mean calculated in Oriana for all cracks measured on all Transect Boulders.

Surface	Modern Wash	Holocene Terrace	Lundy Canyon Outwash Terrace	Lundy Canyon Moraine	Mono Basin Moraine	Buckeye Creek Outwash Terrace	Sherwin Moraine
Surface ID	MW	H1DB	LCTIO	LCTI	LCMB	BCTA	LCSH
Average Surface Area cm <sup>3</sup>	1924	2992	2415	N/A	2070	2373	N/A
Average Rock Length cm	26.6	34.2	28.9	N/A	29.6	32.8	N/A
Average Rock Width cm	17.3	24.4	20.3	N/A	19.2	22.0	N/A
Average Rock Height cm	17.3	10.1	11.2	N/A	8.4	7.5	N/A
Average Crack Length mm	34.8	86.3	58.5	N/A	56.3	59.6	N/A
Average Crack Width mm	0.3	6.9	1.3	N/A	2.7	1.2	N/A
Average Sheet height mm	7.6	5.5	4.3	N/A	8.2	7.5	N/A
Average Crack Density	0.0043	0.0184	0.0122	N/A	0.0052	0.0030	N/A
Strike	136	187	168	N/A	196	164	N/A
Dip	45	46	54	N/A	55	49	N/A

Table 3 continued: Summary table of Transect Boulders and Transect Boulder crack characteristics. Crack Length is the average length of all cracks measured in all Transect Boulders. Crack Width is the average width of all cracks measured in all Transect Boulders.

Sheet height is the average height of the sheet being dislodged by the surface-parallel, measured from all Transect Boulders. Crack Density calculated from the number of cracks on the rock divided by the surface area, then the average was taken from all the Transect Boulders. Crack Strike is the vector mean calculated in Oriana for all cracks measured on all Transect Boulders.

Average Sphericity	3.0	3.1	3.1	N/A	3.1	3.2	N/A
Average Angularity	3.6	3.4	3.4	N/A	2.9	3.6	N/A
Average Weathering Index	4.0	3.5	2.8	N/A	3.3	3.6	N/A
Number of Cracks	21	61	122	N/A	21	13	N/A
Primary Type of Crack	Surface Parallel	Surface Parallel	Un-oriented	N/A	Un-oriented	Un-oriented	N/A

Table 4: Summary table of sample thin section point counts. Sample location refers to which Dated Boulder the sample was taken from. 600 points were sampled on each thin section.

Sample I.D	Sample Location	Age (ka)	Pores	Quartz	Feldspar	Sauserite	Biotite	Unknown	Total
SS2	H1-19	5	9	227	239	123	2	0	600
SS10	LCTIO-2	13.4	10	148	245	192	5	0	600
SS11	LCTIO-1	17	20	157	312	78	33	1	600
SS1	LCTIO-6	17.5	16	261	271	27	18	7	600
SS9	LCTIO-3	17.5	137	144	226	86	7	0	600
SS12 A	LCTIO-4	18.1	15	164	365	56	0	0	600
SS12 B	LCTIO-4	18.1	82	107	268	143	0	0	600
SS7	LCTI-5	18.5	126	116	173	185	0	0	600
SS5	LCMB-3	28.7	31	278	243	47	0	1	600
SS4	LCMB-6	38.9	13	219	193	184	1	0	600
SS3	LCMB -1	43.1	1	221	250	111	17	0	600
SS6	LCMB-2	45.8	26	224	320	29	0	1	600
SS15	BCTA-7	130.4	42	149	62	347	0	0	600
SS14	BCTA-2	150.5	22	242	120	212	0	4	600
SS13	BCTA-1	167.4	146	75	283	85	11	0	600

Table 4 continued: Summary table of sample thin section point counts.

I.D	Lat	Long	% Pores	% Quartz	% Feldspar
SS2	38.0316	119.174092	1.50	37.83	39.83
SS10	38.029382	119.179495	1.67	24.67	40.83
SS11	38.029258	119.179668	3.33	26.17	52.00
SS1	38.030077	119.1761	2.67	43.50	45.17
SS9	38.0294	119.179097	22.83	24.00	37.67
SS12 A	38.029977	119.1752	2.50	27.33	60.83
SS12 B	38.029977	119.1752	13.67	17.83	44.67
SS7	38.026993	119.175183	21.00	19.33	28.83
SS5	38.024877	119.184614	5.17	46.33	40.50
SS4	38.024929	119.184529	2.17	36.50	32.17
SS3	38.024877	119.184614	0.17	36.83	41.67
SS6	38.024877	119.184614	4.33	37.33	53.33
SS15	28.237803	119.316134	7.00	24.83	10.33
SS14	38.237764	119.31854	3.67	40.33	20.00
SS13	38.237886	119.321313	24.33	12.50	47.17



Table 4 continued: Summary table of sample thin section point counts.

% Sausserite	% Biotite	% Unknown	Q/F	abs of 1- Q/F	1/(Q- F)	% Biotite Divided by the sum of % Quartz and % Feldspar
20.50	0.33	0.00	0.95	0.05	50.00	0.00
32.00	0.83	0.00	0.60	0.40	6.19	0.01
13.00	5.50	0.17	0.50	0.50	3.87	0.07
4.50	3.00	1.17	0.96	0.04	60.00	0.03
14.33	1.17	0.00	0.64	0.36	7.32	0.02
9.33	0.00	0.00	0.45	0.55	2.99	0.00
23.83	0.00	0.00	0.40	0.60	3.73	0.00
30.83	0.00	0.00	0.67	0.33	10.53	0.00
7.83	0.00	0.17	1.14	0.14	17.14	0.00
30.67	0.17	0.00	1.13	0.13	23.08	0.00
18.50	2.83	0.00	0.88	0.12	20.69	0.04
4.83	0.00	0.17	0.70	0.30	6.25	0.00
57.83	0.00	0.00	2.40	1.40	6.90	0.00
35.33	0.00	0.67	2.02	1.02	4.92	0.00
14.17	1.83	0.00	0.27	0.73	2.88	0.03

Table 5: Table showing amount of lichen present on boulders on sampled surfaces

	Modern Wash	Holocene Terrace	Tioga Outwash	Mono Basin Moraine	Tahoe Outwash
Lichen 0-30% instances	26	101	170	106	105
Varnish 0-30% instances	66	102	162	100	105

Table 6: Table showing embeddedness of boulders on sampled surfaces

Embeddedness Counts	MW	H1DB	LCTIO	LCMB	BCTA
0	20	0	27	0	0
1	37	13	54	14	6
2	25	20	48	44	41
3	22	89	45	52	72

Table 7: Table showing frequency of each crack type on boulders of sampled surfaces

Crack Type	MW	H1DB	LCTIO	LCTI	LCMB	BCTA	LCSH
Surface	9	27	51	0	11	9	0
Throughgoing	0	6	0	0	1	0	0
Longitudinal	0	4	15	1	4	1	5
Foliation	0	0	3	0	0	0	0
Other	12	24	69	0	26	21	25

Table 8: Table showing the number of instances of each “crack less than 2 cm” value for all seven surfaces, dated and transect boulders both included. “Few” indicates there was less than 1 crack “less than 2 cm”, “Common” indicates there was between 1 and 5 cracks “less than 2 cm”, and “Many” indicates there was more than 5 cracks “less than 2 cm”.

Cracks <2cm	MW	H1DB	LCTIO	LCTI	LCMB	BCTA	LCSH
Few	63	40	52	2	68	33	2
Common	24	46	78	5	31	35	3
Many	17	36	60	0	25	54	7

Table 9: Table showing the number of instances of granular disintegration on the rocks. Data was collected as a binary “yes” or “no”. Granular disintegration refers to loose grain material that was able to be wiped away with a hand on the boulder

Dated Boulders					
Presence of Granular Disintegration	LCTIO	LCTI	LCMB	BCTA	LCSH
Yes	3	0	8	10	4
No	21	10	11	19	10
Transect Boulders					
Presence of Granular Disintegration	MW	H1DB	LCTIO	LCMB	BCTA
Yes	1	4	32	14	29
No	103	118	137	90	72

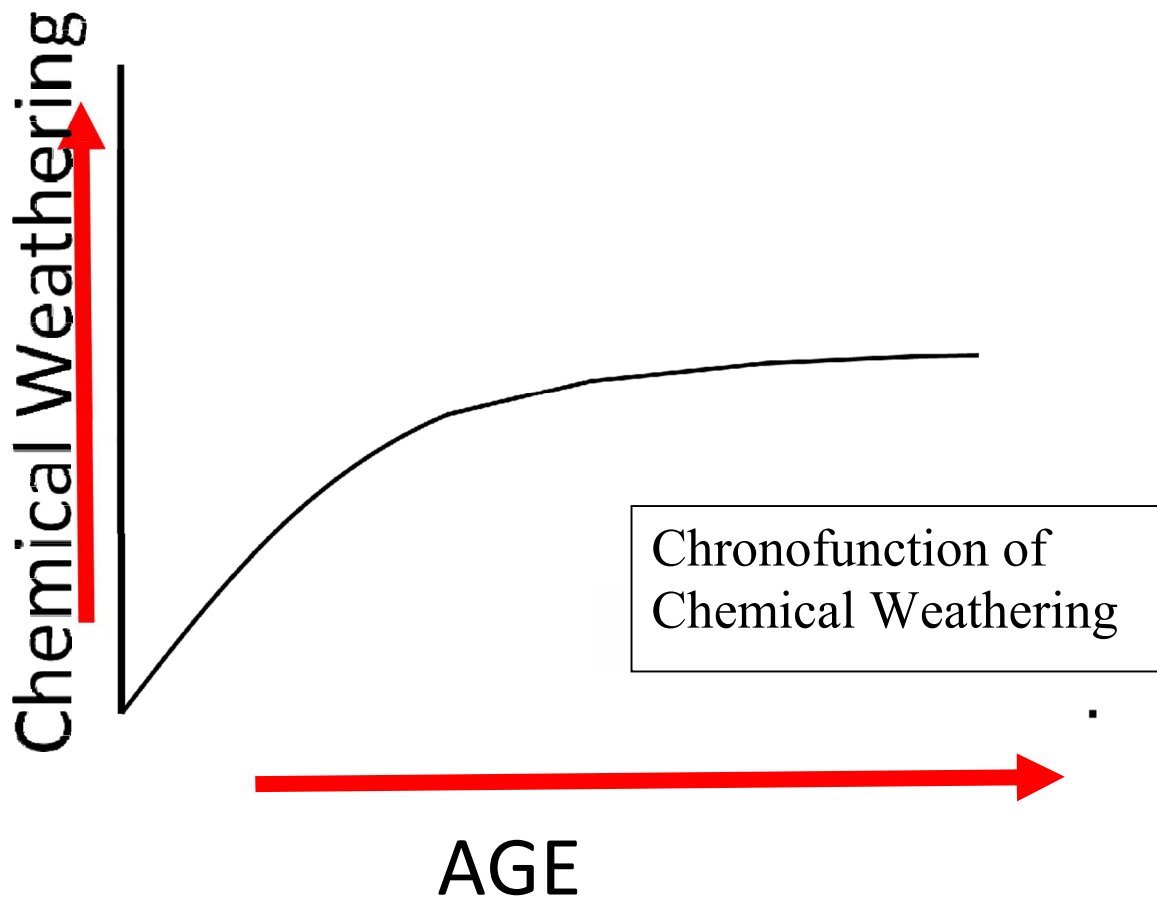


Figure 1: Conceptual graph of chemical weathering over time – derived from numerous chronosequence studies of soil properties (i.e. Birkland, 1999). I hypothesize that a graph for mechanical weathering will look very similar.

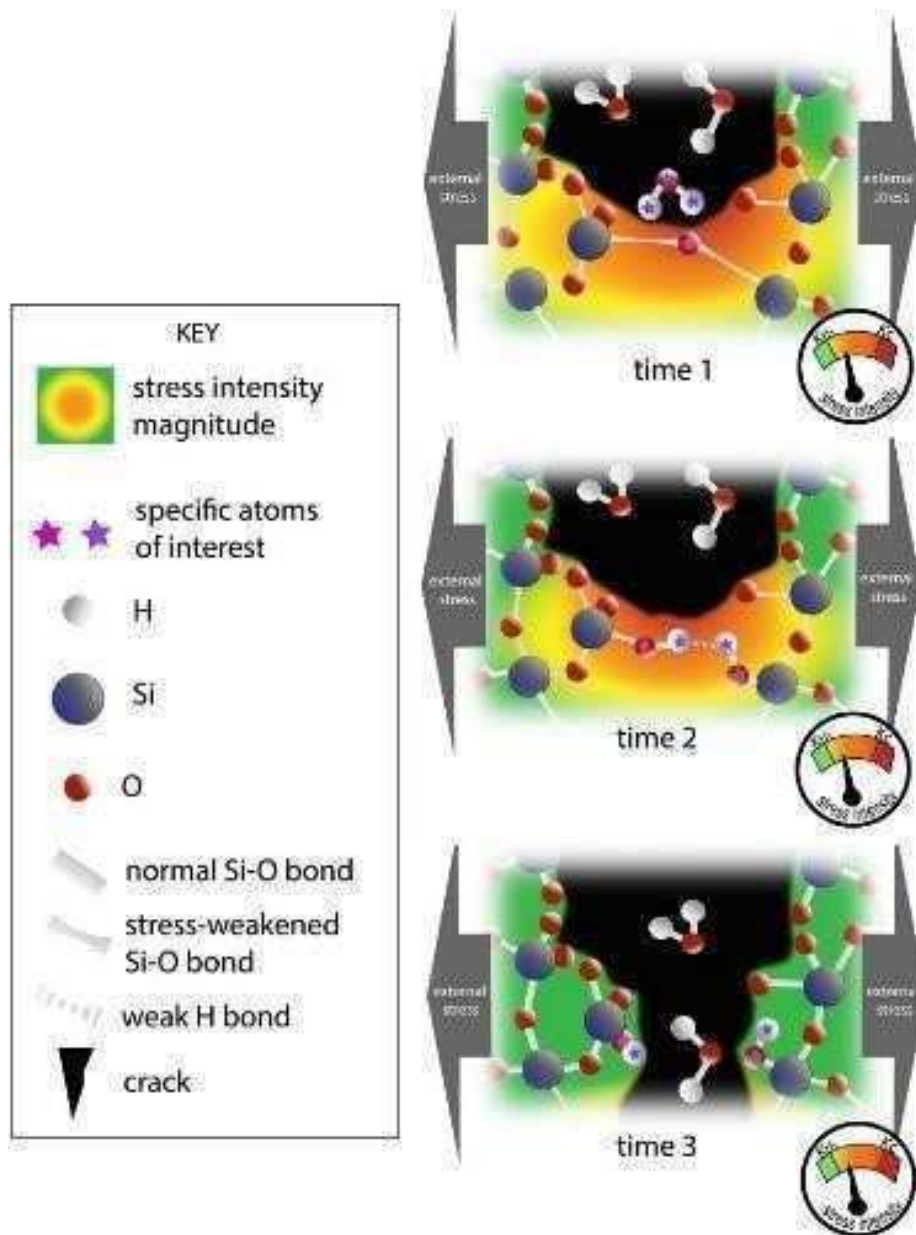


Figure 2: Illustrated Bond Breaking Process. The bond-breaking processes of subcritical cracking occur by chemical reactions between moisture found in the crack, and the rock or mineral itself. Within the rock, the bonds between elements found immediately at the crack tip are experiencing high stress intensity (Time 1). Because of this tension, water molecules become reactive with the mineral or rock, which are weakened at the crack tip, where they are stretched by the stress. This reaction with water replaces the relatively strong bonds of the rock, with weaker hydrogen bonds from the water molecule (Time 2). In that particular location, the breaking of the weaker bonds lead the crack to propagate at stress levels lower than the overall strength of the rock itself (Time 3)

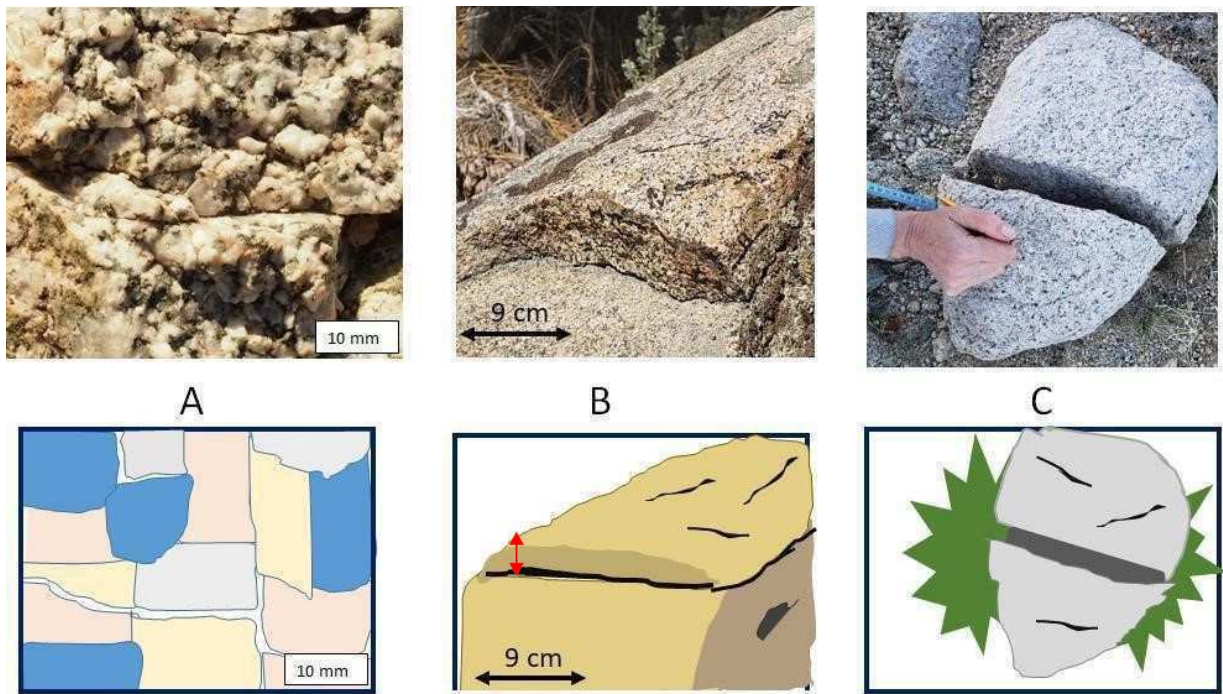


Figure 3: 3 common types of crack morphology. A: Intergranular cracks; form along individual crystal or classic grain boundaries. B: Surface parallel cracks; any crack parallel to the outside boundary of the rock, typically less than 10% of the total height of the rock. C: Through-going cracks; cracks that do not follow any visible boulder related features and will eventually result in the splitting of the rock or boulder into 2 or more pieces.

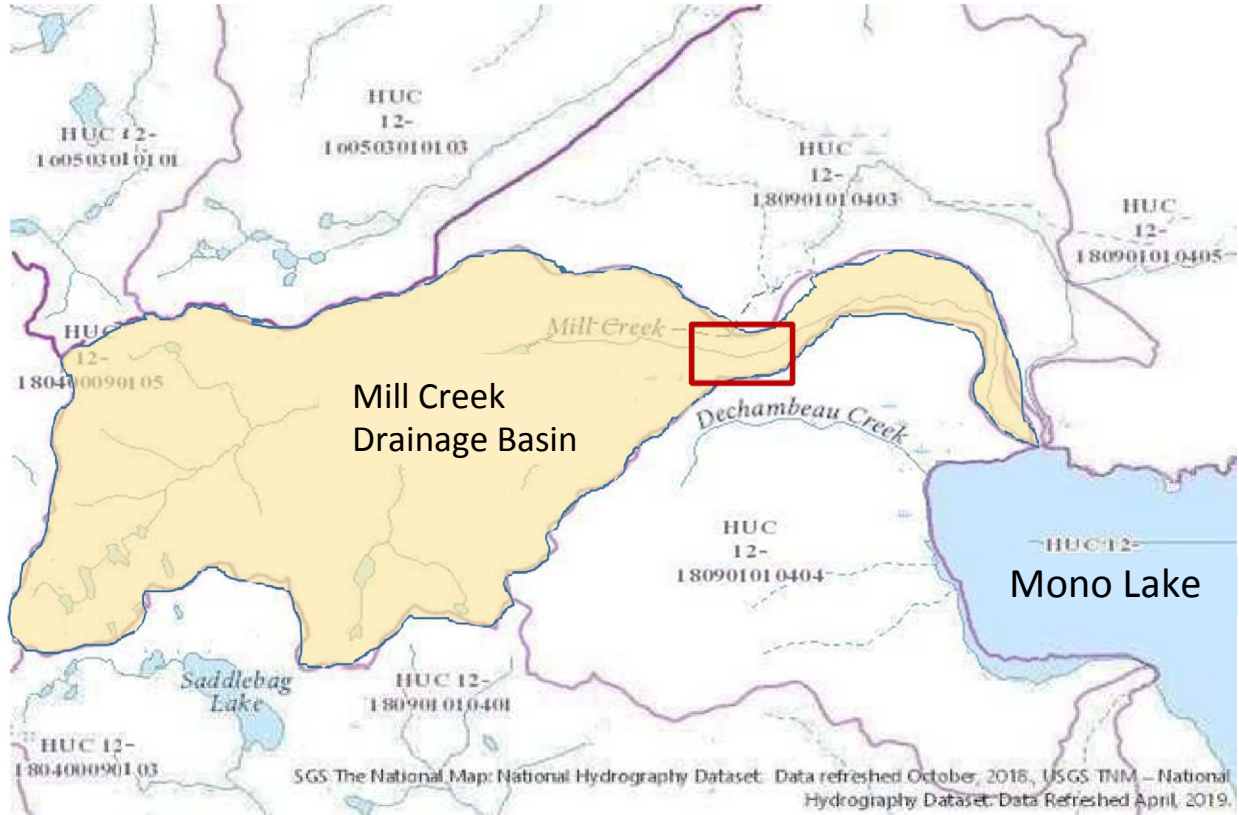


Figure 4: Watershed map from the National Hydrography Dataset showing the extent of the Mill Creek drainage basin. The main field sample sites, marked by the dark red box, were located along Mill Creek.







Figure 5: Map of sample site locations in relation to each other. Buckeye Canyon is outlined in purple, and Lundy Canyon is outlined in yellow. Following figures show sample sites in more detail.

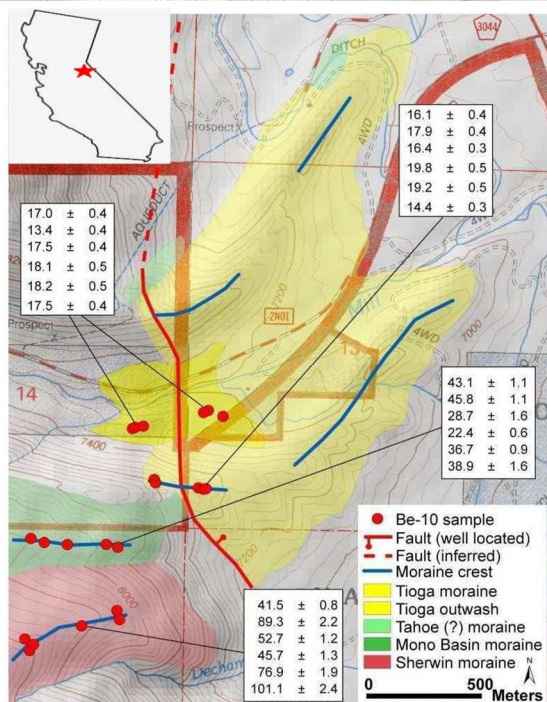
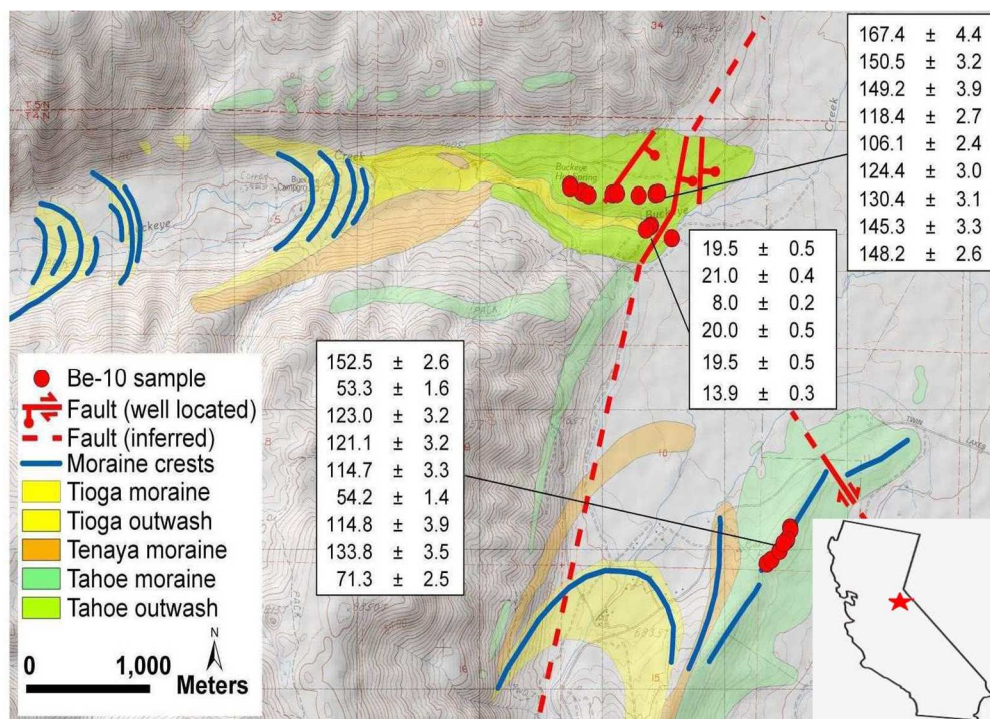


Figure 6: Topographic maps taken from Rood 2011 showing the extent of glacial moraines as well as the Be10 sample sites for both the Lundy and Buckeye areas. The location of these maps is indicated on Figure 2



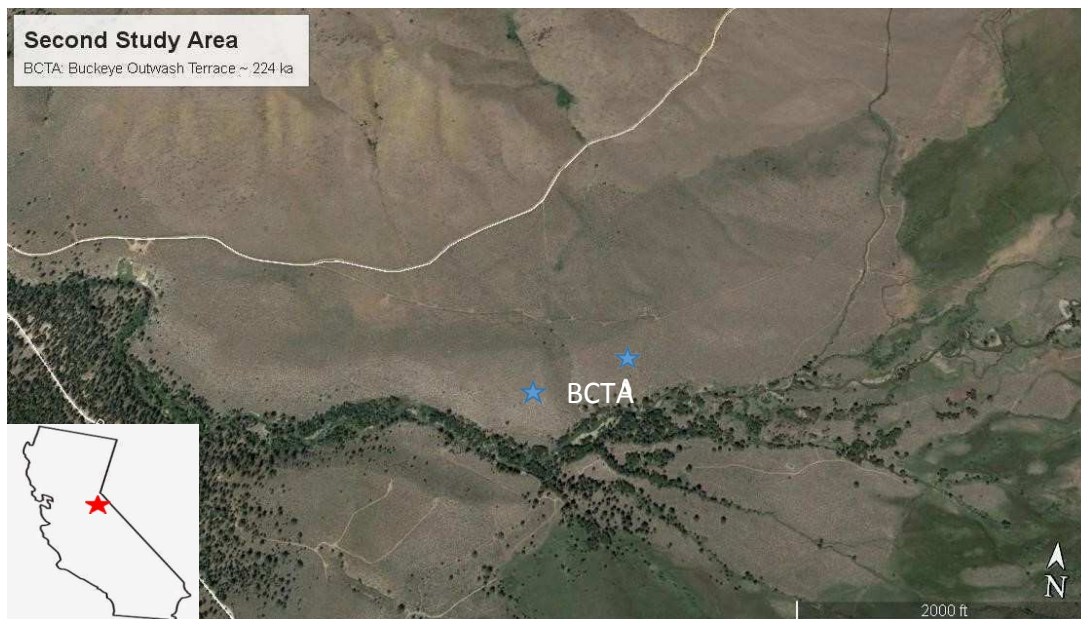
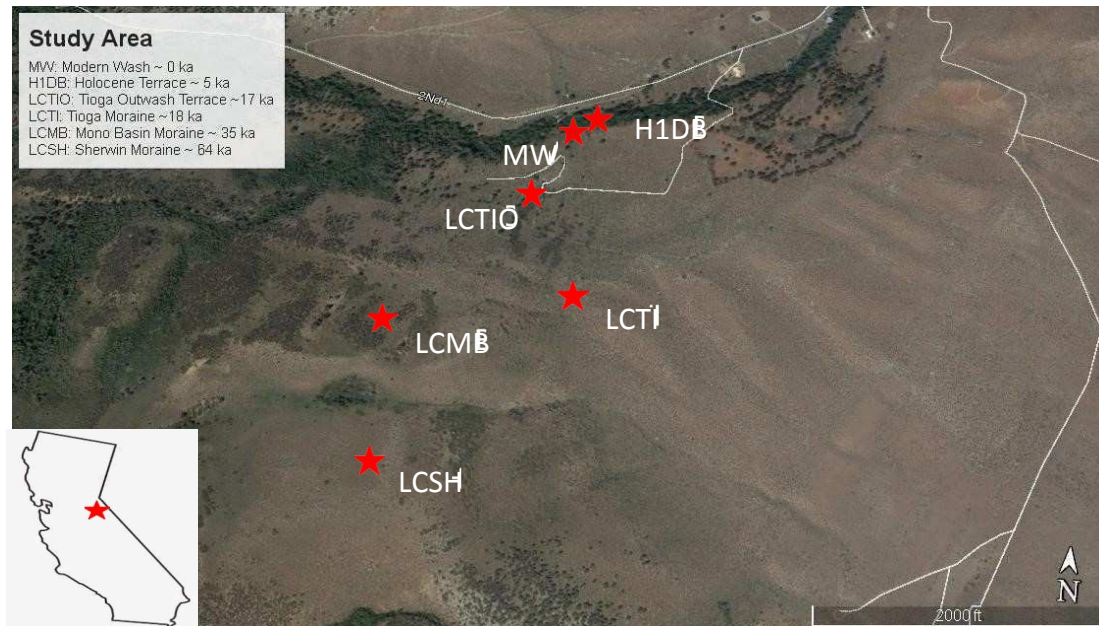


Figure 7: Satellite photos with labels on the surfaces that were sampled in the Berberich 2019 field study



Figure 8: Photos of each sample location. Clockwise from upper left: A: Modern Wash, B: Holocene Terrace, C: Tioga Outwash, Center: Tioga Moraine, D: Sherwin Moraine, E: Buckeye Outwash, F: Mono Basin Moraine.





Figure 9: Example of a dated boulder with a possibly previously sampled area. Evidence of recent rupture, as well as varnish development in the area that was removed. Rite in the rain notebook for scale at the bottom of the figure.

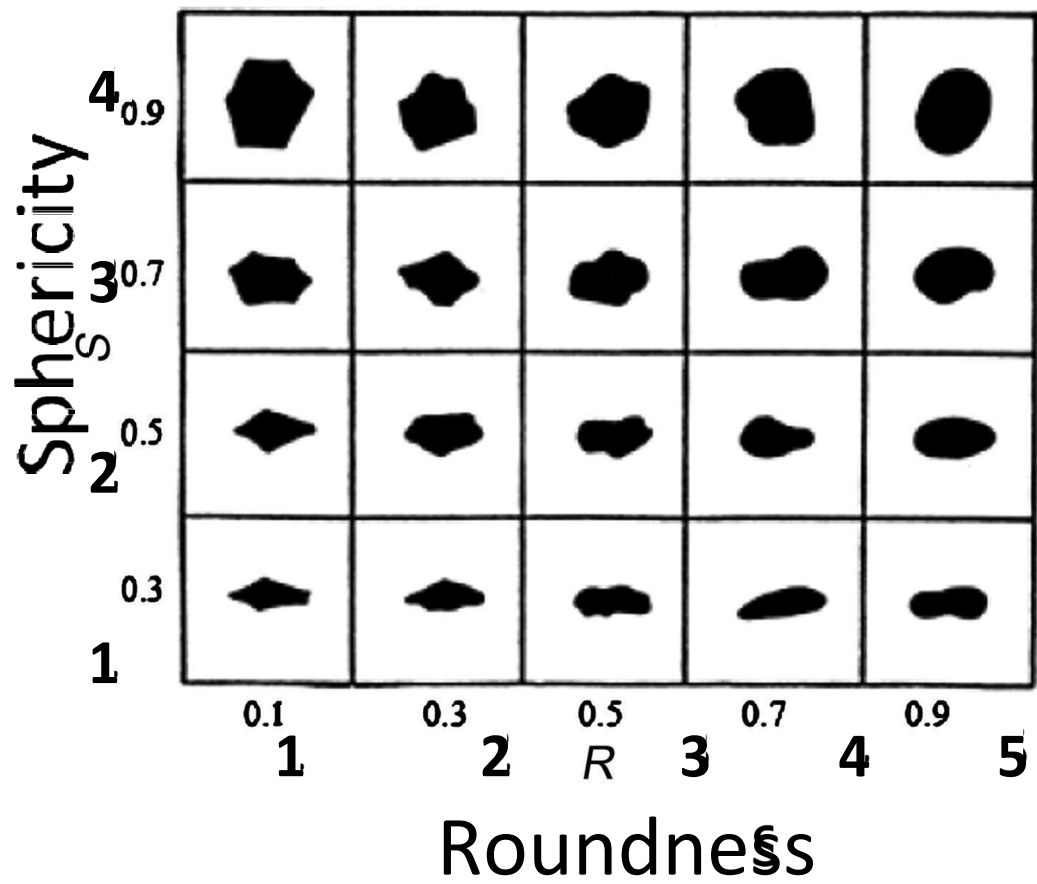


Figure 10: Commonly used chart for sphericity and roundness, scale has been replaced with a custom number set.



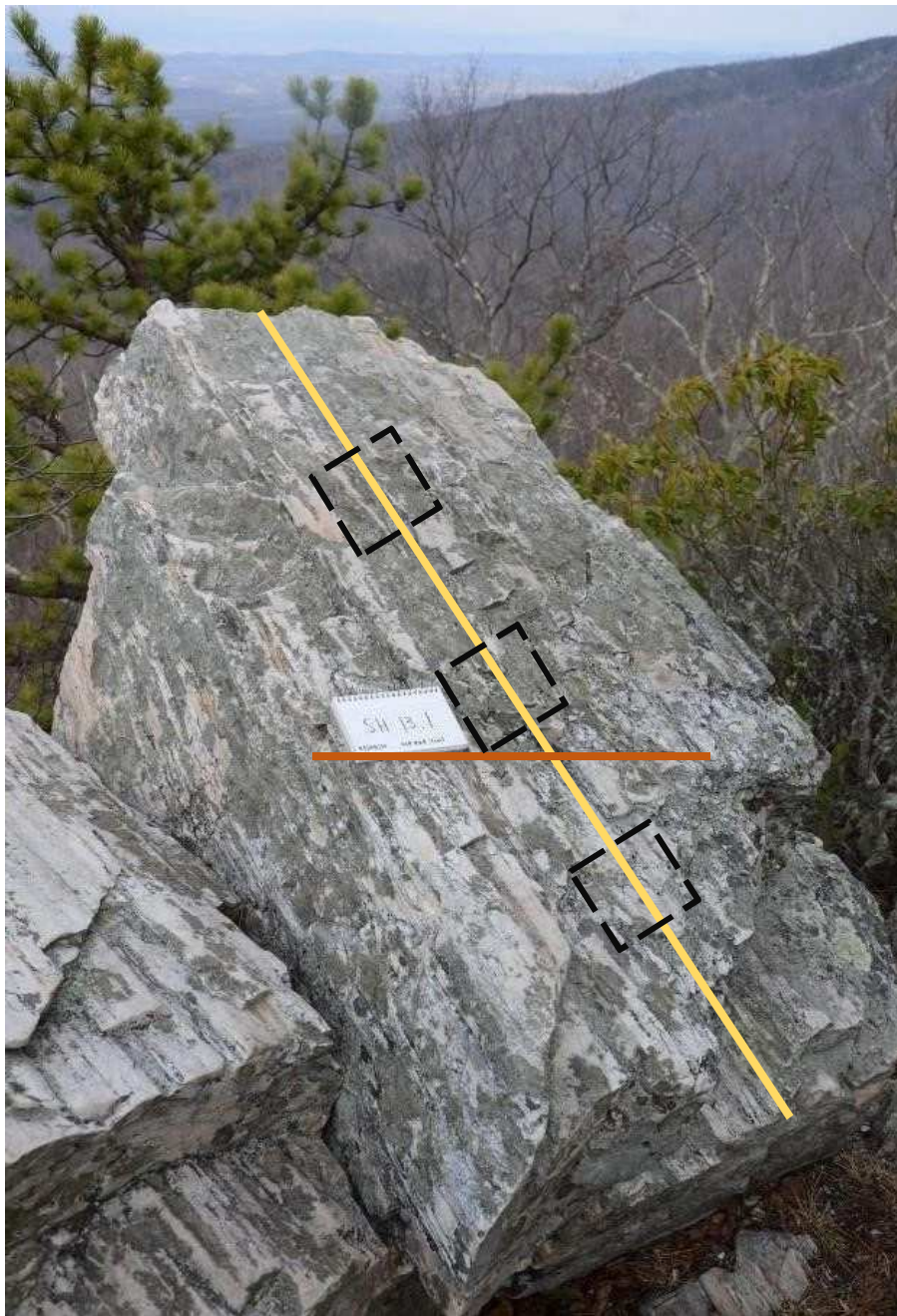


Figure 11: Example of how representative boxes were placed on boulders. Orange line indicates the width of the boulder, creating a midpoint for the length of the boulder to be measured. Yellow line indicates the length of the boulder, measured along the midpoint. Based on the size of the boulder in question, between 2 and 4 representative boxes would be drawn. Rite in the Rain field notebook for scale. Outcrop pictured is in Shenandoah National Park.

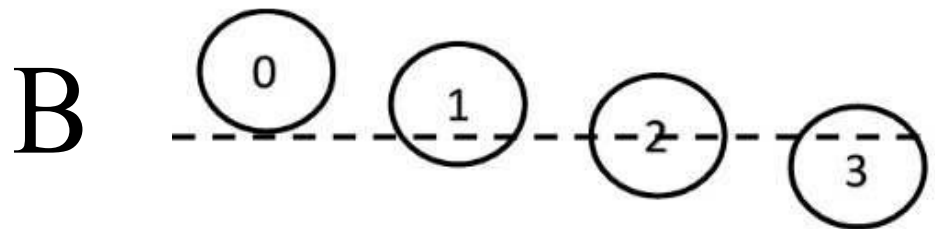
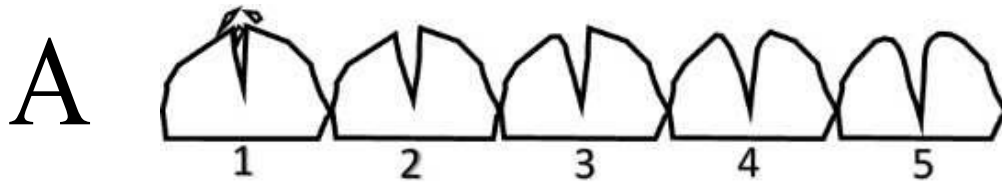


Figure 12: A: Embeddedness scale for boulders, and B: Crack weathering index. Diagrams created by Stephen Porson (2020)



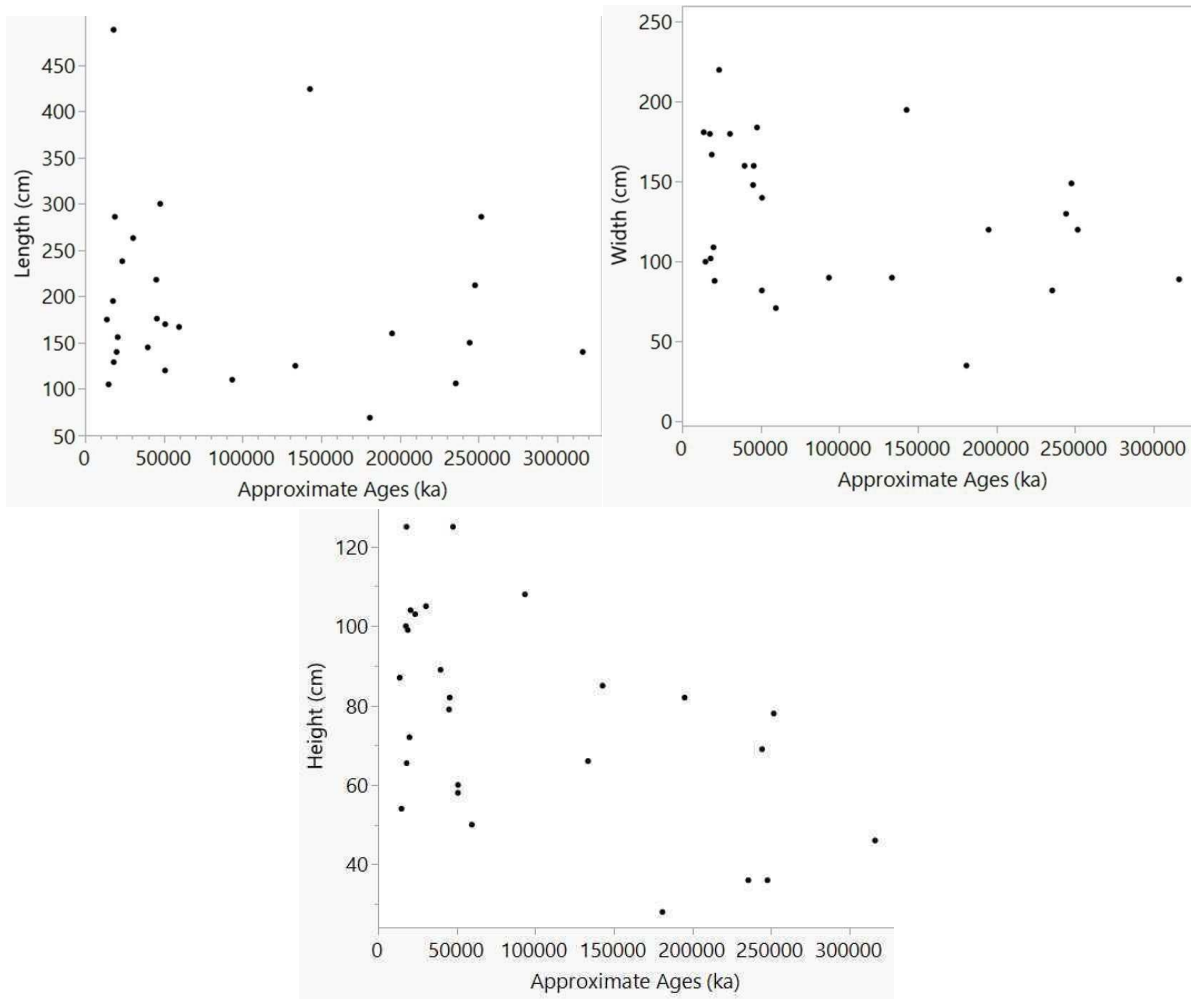


Figure 13: Dimensions of Dated Boulders based on Approximate Ages. There is a general trend that shows a decrease in the dimensions of the dated boulders as the surfaces they are located on get older

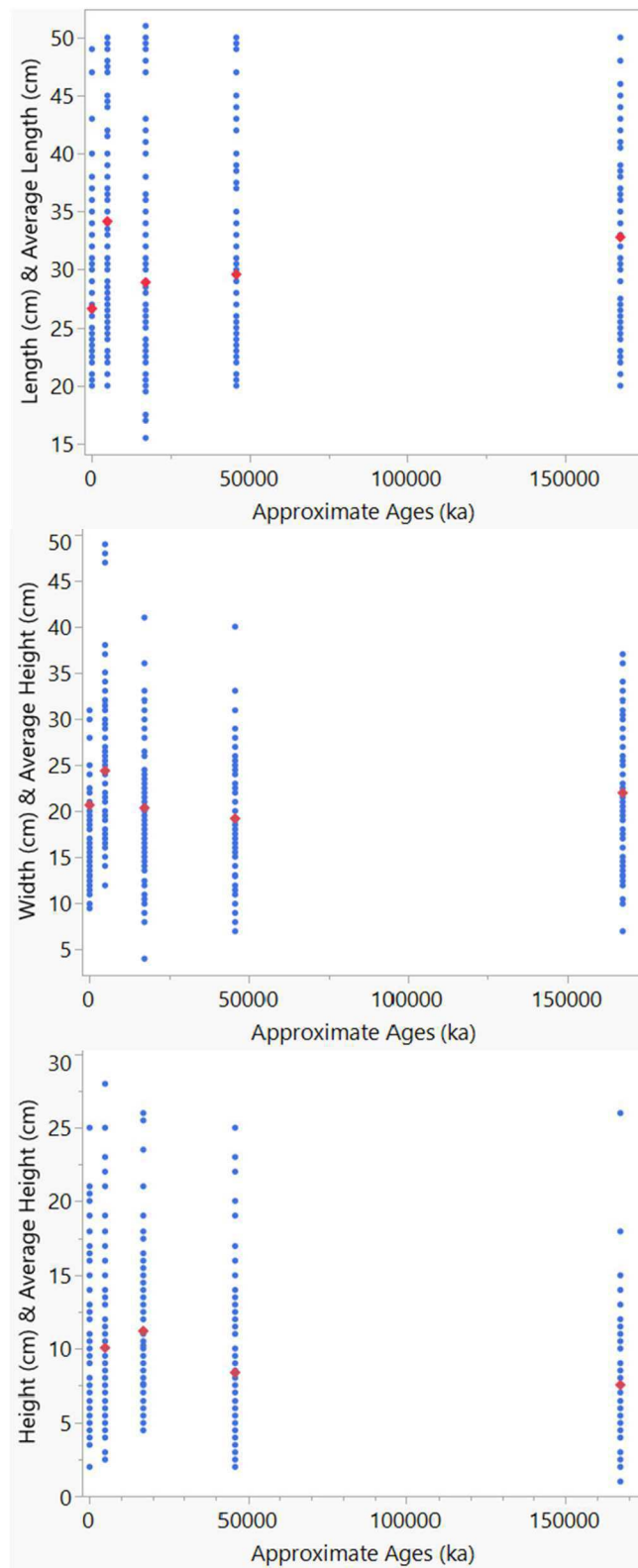


Figure 14: Dimensions of Transect Boulders Based on Approximate Ages. A positive relationship can be seen between the ages of the surface and the length and width of transect boulders. A reverse relationship can be seen in regards to the height of the transect boulders decreasing with time

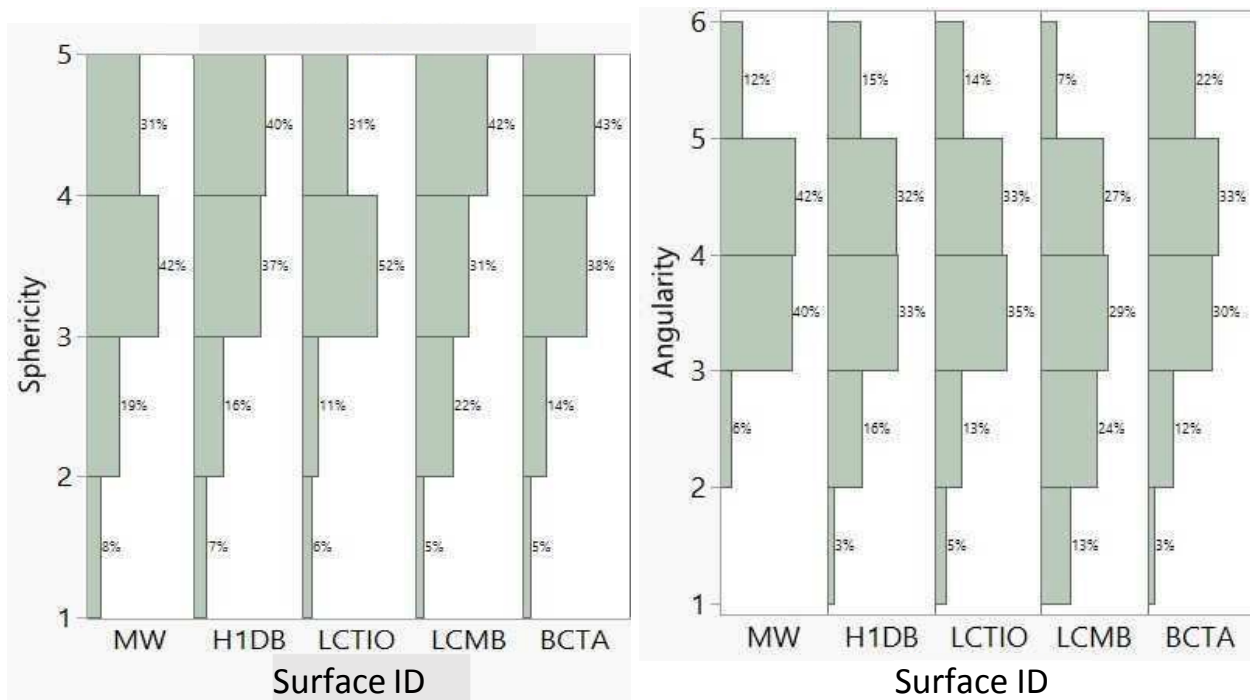


Figure 15: Sphericity and Angularity of transect boulders for each Surface. A) Modern Wash, B) Holocene Terrace, C) Tioga Outwash Terrace, D) Mono Basin Moraine, E) Tahoe Outwash Terrace. Tioga Moraine and Sherwin Moraines were excluded due to no transects being done there. The higher the sphericity value, the more round the boulder is. The higher the angularity value, the “sharper” the boulder is.

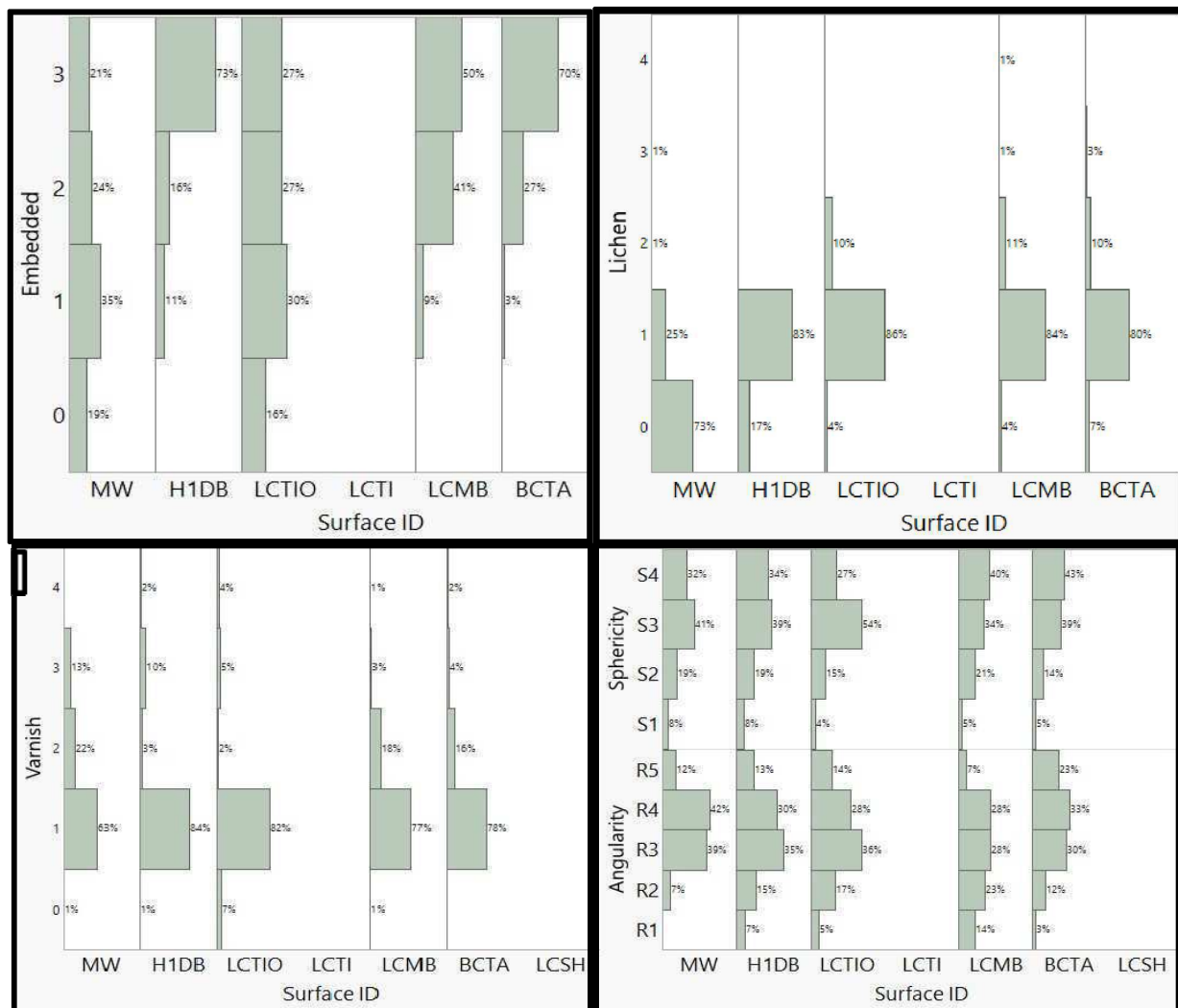


Figure 16: Quadruple graph of percent embeddedness, percent sphericity/angularity, percent varnish, and percent lichen of boulder transects over time.

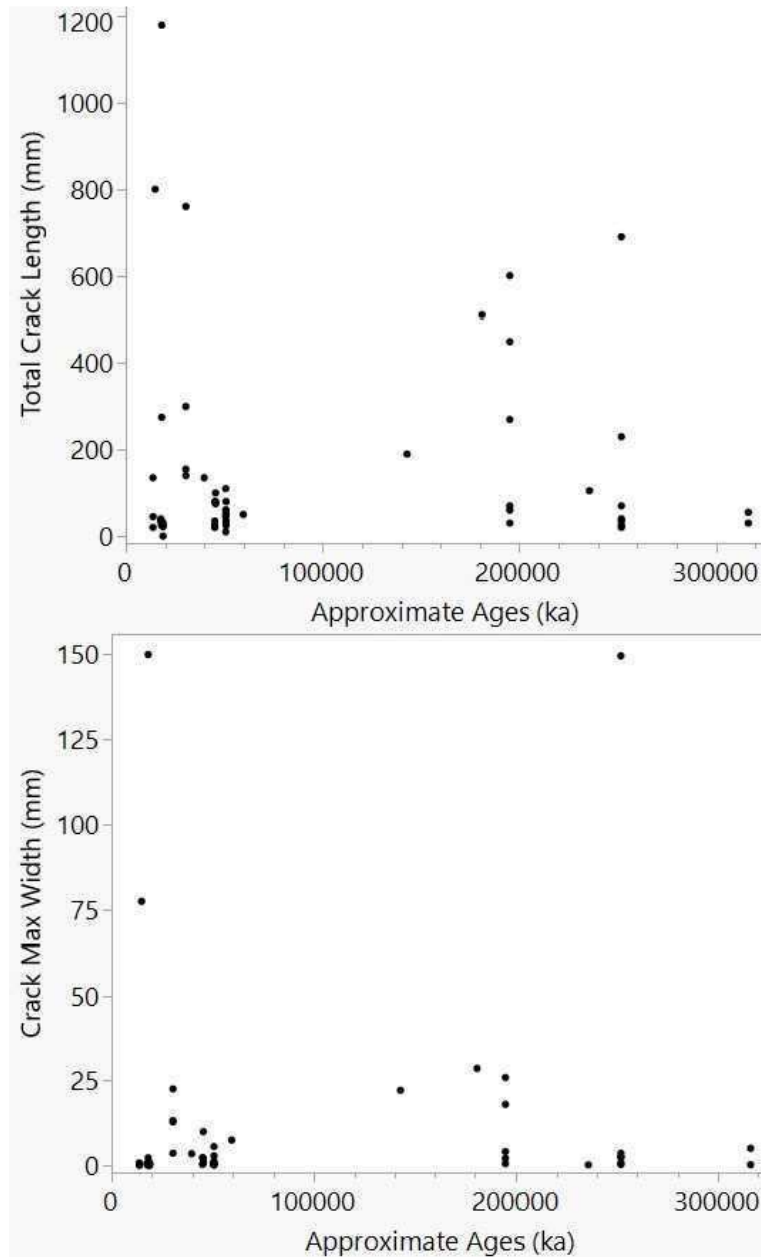


Figure 17: Crack Dimensions for Dated Boulders. A slight positive trend can be seen between the crack dimensions on dated boulders and the age of the surface the boulders are located on.

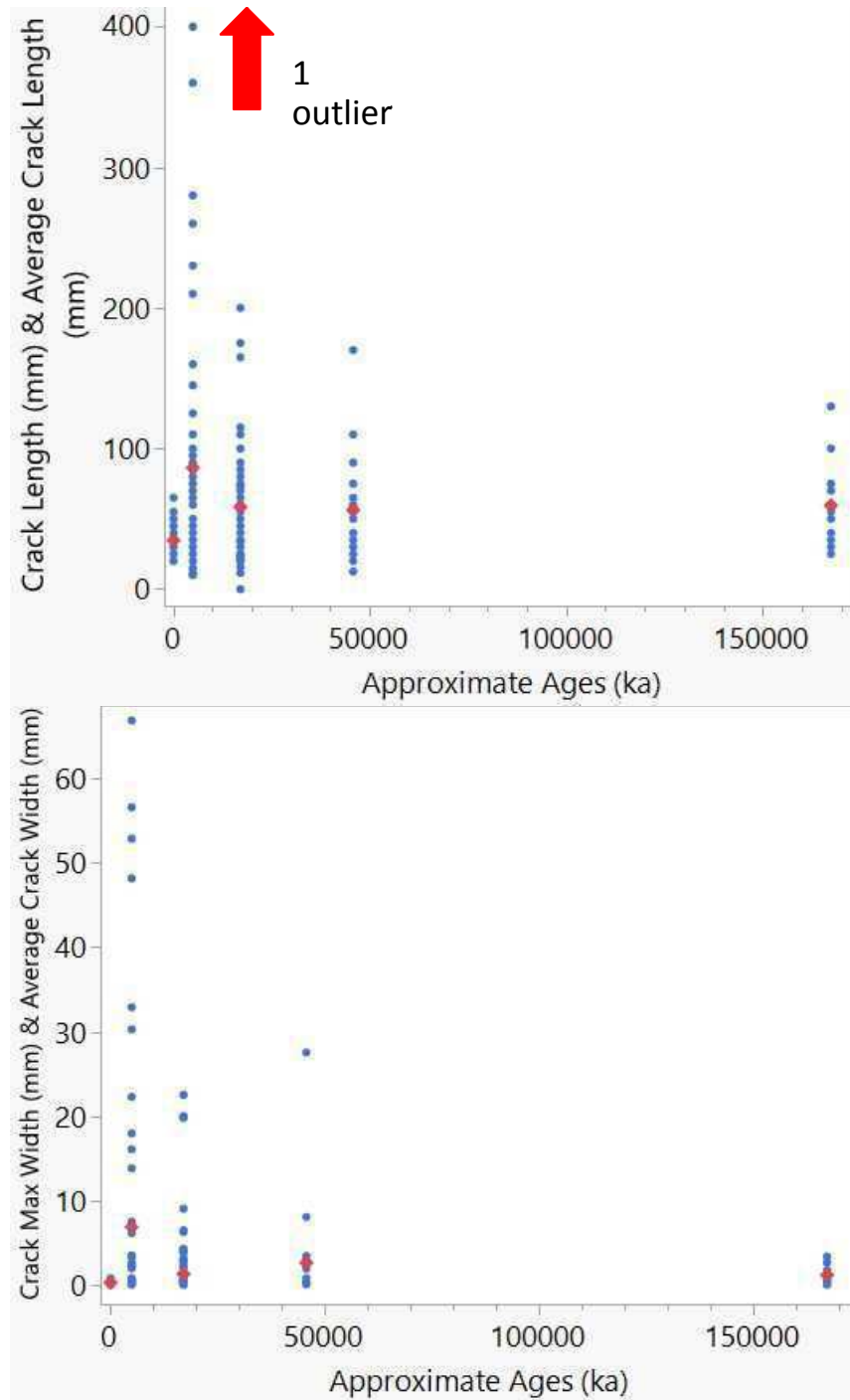


Figure 18: Crack Dimensions for Transect Boulders. A slightly negative relationship can be seen between crack dimensions on transect boulders and the age of the surfaces the transect boulders are located on. Outlier (17100 ka, 850 cm) was not excluded from analysis

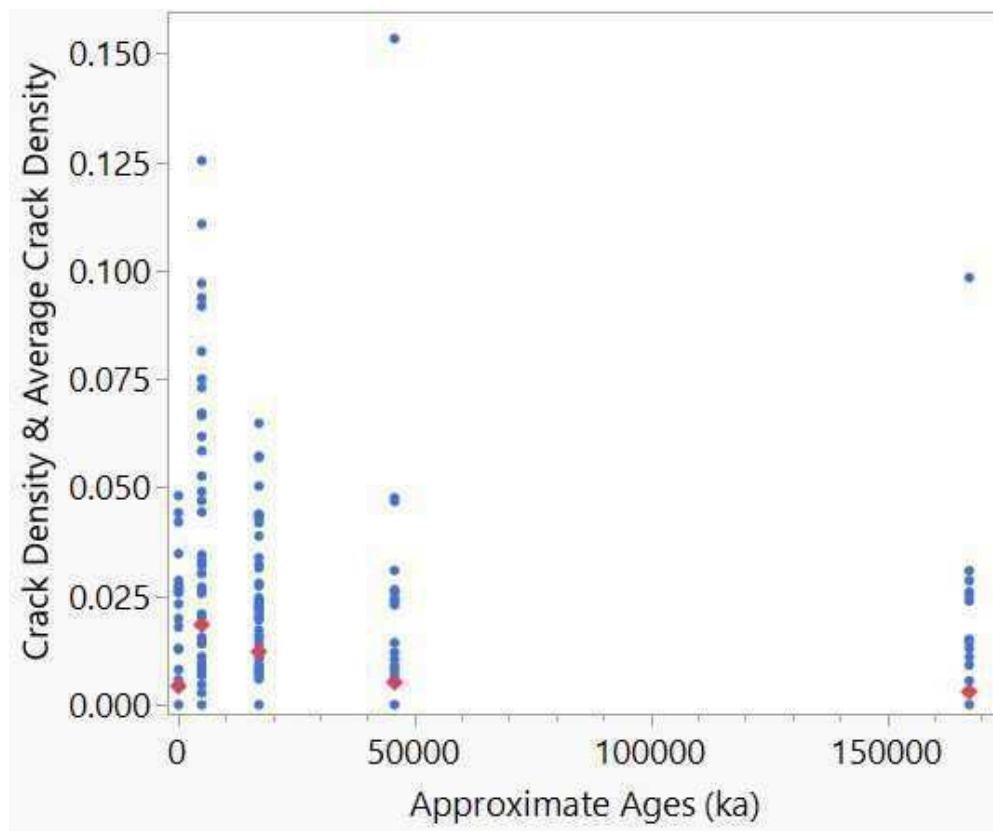


Figure 19: Crack Density and Average Crack Density over Time of Transect Boulders. Crack density for transect boulders on each surface is marked in blue, while the average crack density per surface is marked in red. There is a spike in crack densities around 5000 ka, followed by a slow decline and eventual plateau.

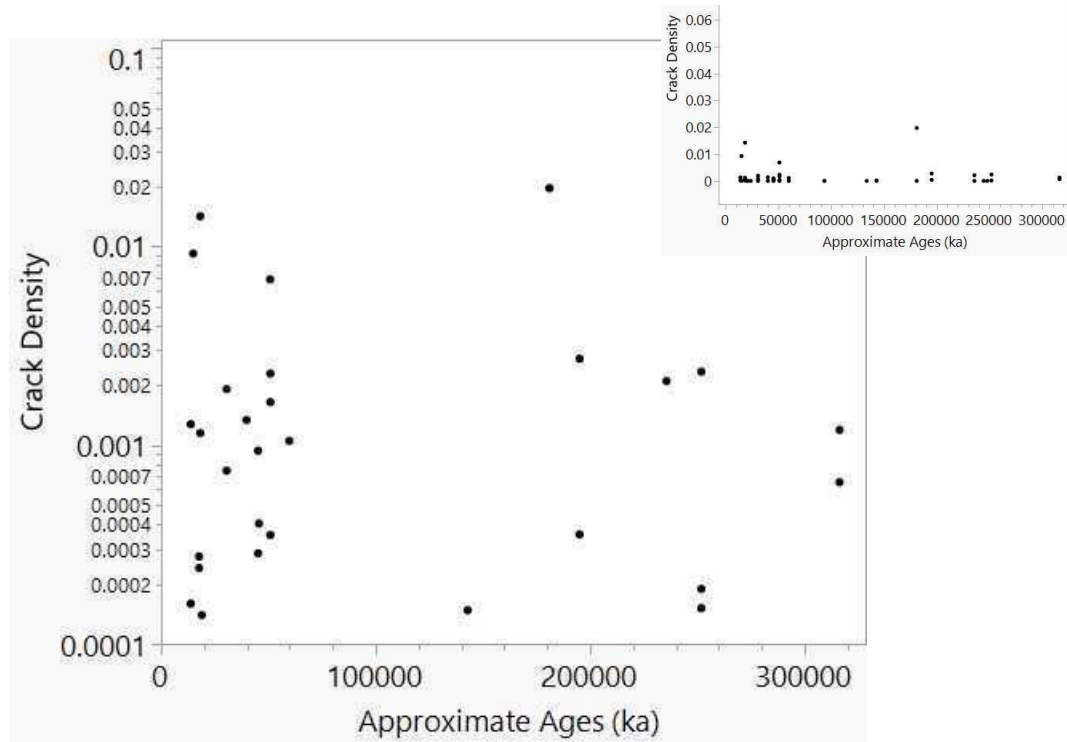


Figure 20: Log of Crack Density vs Age of Dated Boulders.

Log scale scatter plot of crack densities for all dated boulders based on approximate age, not necessarily surface. A slight positive relationship between crack density and age of dated boulders can be seen, however, with the data logged, the relationship could be skewed slightly.

Inset shows range of crack density when Y axis is not logged.



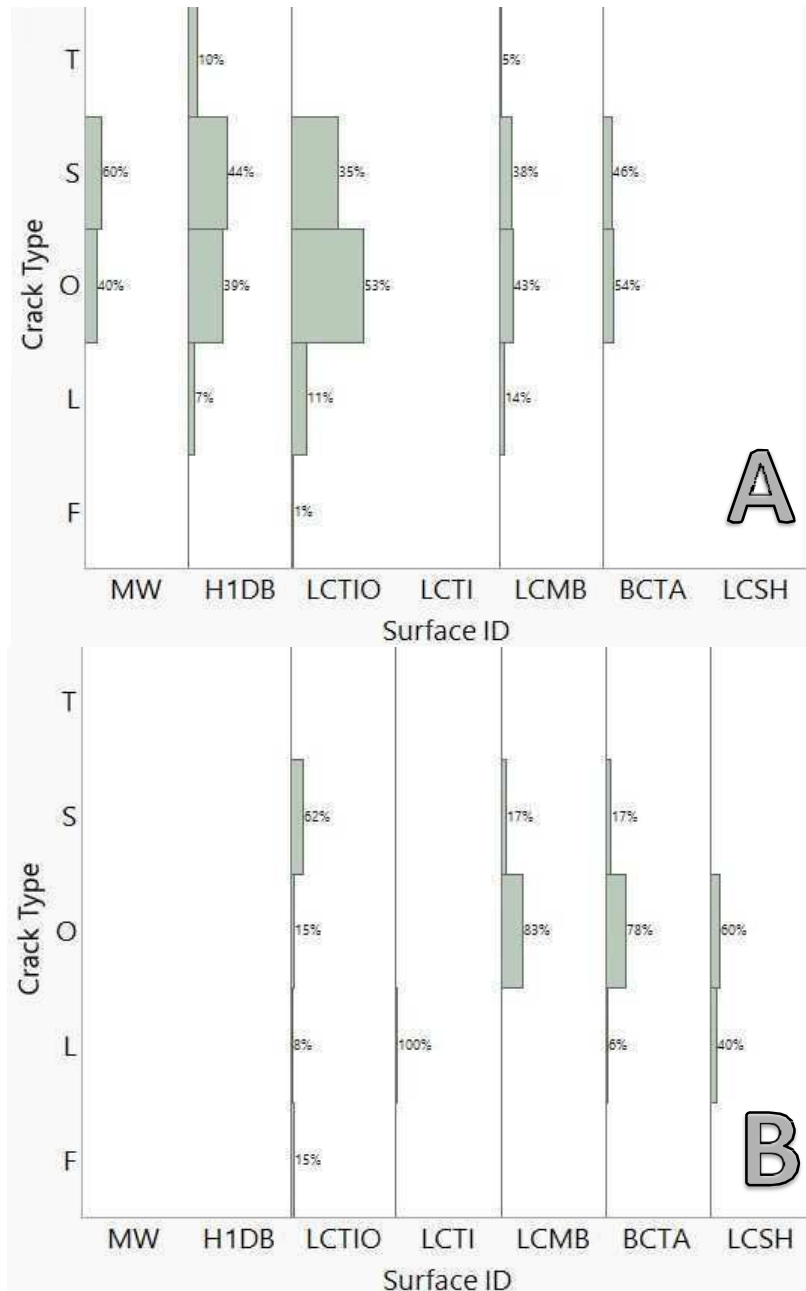


Figure 21: A) Percentage of each crack type present on surfaces with boulder transects. B) Percentage of each crack type present on surfaces with dated boulders. Crack types: T – Through- going, S – Surface, O - Other, L- Longitudinal, F - Fabric

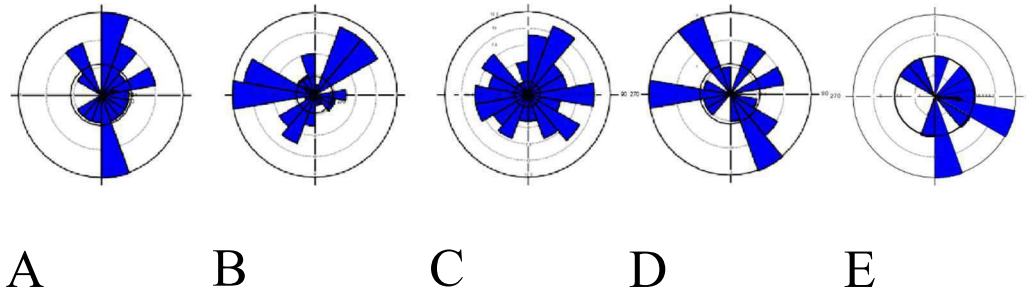


Figure 22: Rose diagrams of all strikes of transect boulders. A) Modern Wash, B) Holocene Terrace, C) Tioga Outwash Terrace, D) Mono Basin Moraine, E) Tahoe Outwash Terrace. No distinct pattern is seen between all five surfaces, however, surfaces B and C, exhibit similar NE/SW strikes, and surfaces D and E exhibit similar NW/SE strikes.

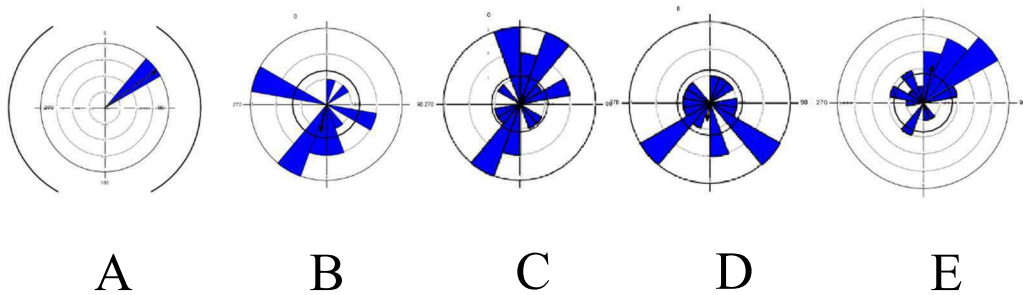


Figure 23: Rose diagrams of all strikes of dated boulders. A) Tioga Moraine, B) Tioga Outwash Terrace, C) Mono Basin Moraine, D) Tahoe Outwash Terrace, E) Sherwin Moraine. No distinct pattern of trendlines can be seen on cursory examination

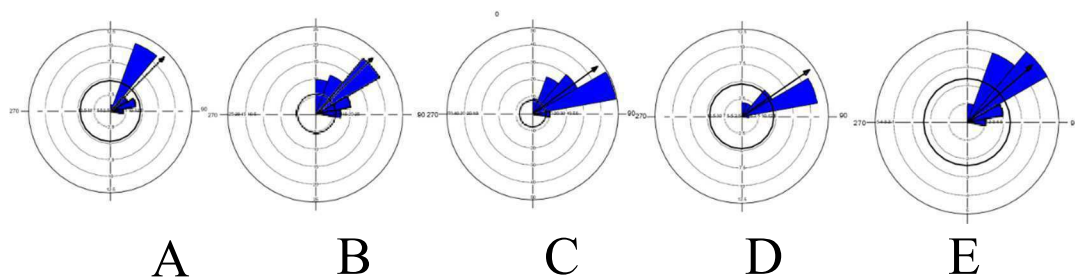


Figure 24: Rose diagrams showing the trend in dips for transect boulders based on surface. All the surfaces have a NE trending dip. Modern Wash, B) Holocene Terrace, C)Tioga Outwash Terrace, D) Mono Basin, E) Tahoe Outwash Terrace

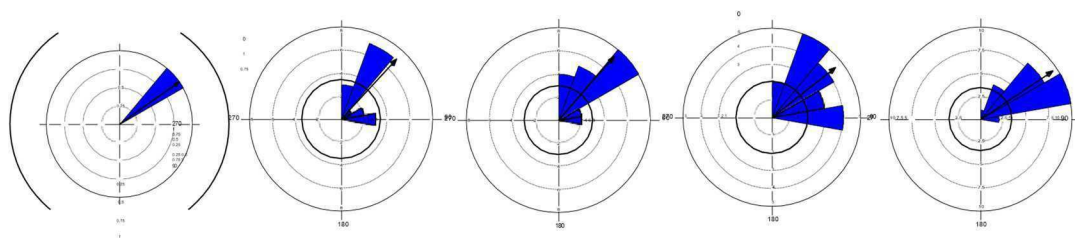


Figure 25: Rose diagrams showing the trend in dips for dated boulders based on surface. All the surfaces have a NE trending dip. A) Tioga Moraine, B) Tioga Outwash Terrace, C) Mono Basin Moraine D) Tahoe Outwash Terrace, E) Sherwin Moraine

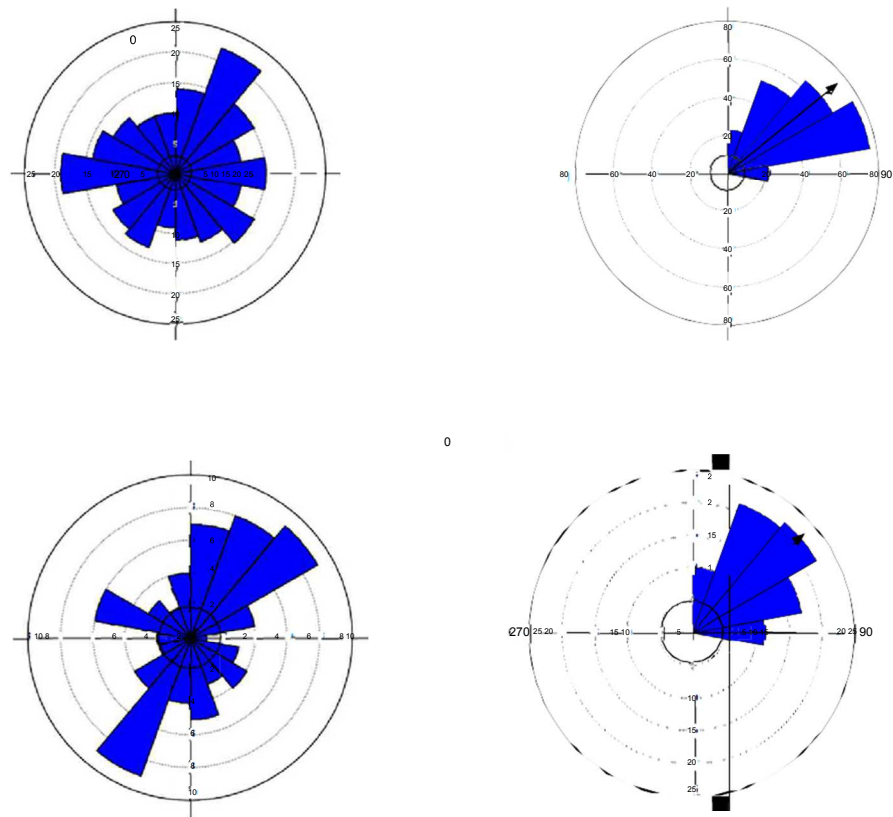


Figure 26: Average crack strike (A) and dip (B) for transect boulders, and average crack strike(C) and dip (D) for dated boulders. All have a NE/SW trend





Figure 27: Example of a “daughter boulder” on the Tioga Outwash surface. Name taken from the lexicon of isotopes.